universität wien

MASTERARBEIT / MASTER'S THESIS

Titel der Masterarbeit / Title of the Master's Thesis

Metallomic approaches for the analysis of metallodrugs in biological systems

verfasst von / submitted by

Elisabeth Föls, BSc

angestrebter akademischer Grad / in partial fulfilment of the requirements for the degree of

Master of Science (MSc)

Wien, 2021 / Vienna 2021

Studienkennzahl lt. Studienblatt / degree programme code as it appears on the student record sheet:	A 066 862
Studienrichtung lt. Studienblatt / degree programme as it appears on the student record sheet:	Master Chemie
Betreut von / Supervisor:	Univ.– Prof. Dr. Gunda Köllensperger
Mitbetreut von / Co-Supervisor:	Mag. Dr. Sarah Theiner

Acknowledgments

At first, I would like to thank Gunda Köllensperger for her supervision and the opportunity to acquire new abilities.
Furthermore, I would like to thank Sarah Theiner and especially Andreas Schweikert for their constant support and the numerous explanations of the instruments. Thank you for taking the time to demonstrate everything to me and answer my questions.
A big thank you also goes to Sophie Neumayer for explaining the digestion procedure to me and for the help with the data evaluation.
Basically, I want to thank the whole group for the friendly atmosphere.

I want to thank Dina Baier for providing the samples and the biological matrices.

My sincere gratitude also goes to Anna Fabisikova and Martin Zehl for the measurements in the mass spectrometry centre and the assistance with the data evaluation.

I would also like to thank my family without whose help it would not have been possible to complete my degree.

Abstract

Cancer is one of the most common causes of death. In the process, body cells change and continue to grow uncontrollably, damaging the surrounding tissue. As the disease progresses, the cancer can spread further by forming metastases. Numerous diseases are subsumed under the umbrella term cancer. The treatments are not trivial and there are often undesirable side effects, which further burden the quality of life of those affected.
Therefore, the need for research and development of new anticancer drugs is essential. The focus is on a targeted treatment of the affected region and the side effects must be as low as possible.

The aim of this study was investigation of the behaviour of the metal-based anticancer drug KP1339 in different biological systems, based on inductively coupled plasma-mass spectrometry (ICP-MS). Therefore, size exclusion chromatography methods in combination with ICP-MS were carried out to analyse the protein binding kinetics and the stability of KP1339. For the investigation of the kinetics of the protein binding, the metallodrug was incubated in different biological matrices (cell medium, serum, buffer, ..) and the samples were measured at different time points. The influence of different solvents on the kinetics was also examined.
In addition to ICP-MS-based methods, measurements were also carried out in the field of organic mass spectrometry. Based on the results of the measurements with ICP-MS, targeted samples were analysed with an orbitrap in combination with reversed-phase chromatography. The additional results successfully showed that not only protein binding to albumin occurs. However, various other compounds, which were developed over time could be proved.

The Medical University of Vienna provided *in vivo* samples (serum and blood pellet) of mice treated with KP1339 and etomoxir + KP1339. The ruthenium content could be determined for both sample types with ICP-MS. For the serum samples, additional measurements were performed with SEC-ICP-MS. This allowed the binding of KP1339 to albumin to be investigated.

Zusammenfassung

Krebserkrankungen sind eine der häufigsten Todesursachen. Dabei verändern sich Körperzellen und wachsen unkontrolliert weiter und schädigen dadurch das umliegende Gewebe. Bei fortschreitender Erkrankung kann sich der Krebs durch Bildung von Metastasen weiter ausbreiten. Unter dem Oberbegriff Krebs werden zahlreiche Erkrankungen subsumiert. Die Behandlungen sind nicht trivial und es treten oft unerwünschte Nebenwirkungen auf, welche die Lebensqualität der Betroffenen weiter belasten.

Daher ist der Bedarf an Forschung und Entwicklung neuer Krebsmedikamente unabdingbar. Der Fokus liegt dabei auf einer gezielten Behandlung der betroffenen Region im Körper, wobei die Nebenwirkungen so gering wie möglich gehalten werden sollten.

Ziel dieser Studie war es, verschiedene Messungen des metallbasierten Krebsmedikaments KP1339 auf Basis der induktiv gekoppelten Plasma-Massenspektrometrie (ICP-MS) durchzuführen. Dazu wurden Größenausschluss-Chromatographie-Methoden in Kombination mit ICP-MS durchgeführt, um die Proteinbindungskinetik und die Stabilität von KP1339 zu analysieren. Zur Untersuchung der Kinetik der Proteinbindung wurde KP1339 in verschiedenen biologischen Matrices (Zellmedium, Serum, Puffer, ..) inkubiert und die Proben zu verschiedenen Zeitpunkten gemessen. Auch der Einfluss verschiedener Lösungsmittel auf die Kinetik wurde untersucht.

Zusätzlich zu diesen Messungen wurden auch Messungen im Bereich der organischen Massenspektrometrie durchgeführt. Basierend auf den Ergebnissen der Messungen mit ICP-MS wurden gezielte Proben mit einer Orbitrap in Kombination mit Umkehrphasen-Chromatographie analysiert. Die zusätzlichen Ergebnisse zeigten erfolgreich, dass nicht nur eine Proteinbindung an Albumin stattfindet. Vielmehr konnten verschiedene Verbindungen, die im Laufe der Zeit entstanden sind, nachgewiesen werden.

Die Medizinische Universität Wien stellte *in vivo* Proben (Serum und Blutpellet) von Mäusen zur Verfügung, die mit KP1339 und Etomoxir + KP1339 behandelt wurden. Der Rutheniumgehalt konnte für beide Probentypen mit ICP-MS bestimmt werden. Für die Serumproben wurden zusätzlich Messungen mit SEC-ICP-MS durchgeführt, wodurch die Bindung von KP1339 an Albumin untersucht werden konnte.

List of abbreviations

AA	Amino acid
AC	Alternating current
ACN	Acetonitrile
Ar	Argon
BEH	Ethylene bridged hybrid
BSA	Bovine serum albumin
CAS	Chemical abstract service
CE	Capillary electrophoresis
Ce	Cerium
Cl	Chlorine
CID	Collision-induced dissociation
Co	Cobalt
CoA	Coenzyme A
Conc.	Concentration
CPS	Counts per second
CRC	Collison-reaction cell
DC	Direct current
DMSO	Dimethyl sulfoxide
ESI	Electrospray ionization
FA	Formic acid
FCS	Fetal calf serum
FFBSA	Fat free bovine serum albumin
FT	Fourier transformation
GC	Gas chromatography
HAc	Acetic acid
HCl	Hydrogen chloride
HNO_3	Nitric acid
HPLC	High performance liquid chromatography
H_2O	Water
H_2O_2	Hydrogen peroxide
HSA	Human serum albumin

ICP	Inductively coupled plasma
ICP-MS/MS	Inductively coupled plasma triple quadrupole mass spectrometry
In	Indium
i.p	Intraperitoneal injection
i.v	Intravenous injection
L	Indazol ($C_7H_6N_2$)
LC	Liquid chromatography
Li	Lithium
LOQ	Limit of quantification
MALDI	Matrix assisted laser desorption/ionization
MC	McCoy medium
MC10	McCoy medium + 10% FCS
MC10delip.	McCoy medium + 10% FCS; delipidated
MeOH	Methanol
mM	Millimolar
MQ	M-Clarity^{TM} quality level
MS	Mass spectrometry
m/z	Mass-to-charge ratio
NaCl	Sodium chloride
NH_3	Ammonia
NH_4Ac	Ammonium acetate
Ni	Nickel
KED	Kinetic energy discrimination
KP1019	Indazolium *trans*-[tetrachloridobis (1H-indazole) ruthenate(III)]
KP1339	Sodium *trans*-[tetrachloridobis (1H-indazole) ruthenate(III)]
O_2	Oxygen
OA BSA	Oleic acid bovine serum albumin
P	Phosphorus
PBS	Phosphate-buffered saline
PFA	Perfluoroalkoxy alkane
ppb	Parts per billion
ppm	Parts per million

ppt	Parts per trillion
QQQ	Triple quadrupole mass spectrometer
ReTOF	Reflectron time-of-flight mass spectrometry
RF	Radio frequency
RP	Reversed-phase chromatography
Ru	Ruthenium
RT	Retention time
r.t.	Room temperature
S	Sulphur
SEC	Size-exclusion chromatography
SQ mode	Single quadrupole mode
Tl	Thallium
TOF	Time-of-flight
TRA	Time resolved analysis
V	Volume
Y	Yttrium

Table of Contents

1 Introduction

1.1 Cancer: An overview

Chemotherapy is one of the most important treatment options for malignant tumours, along with surgery and radiation therapy. [1] Platinum-based anticancer drugs are widely used. However, some undesirable side effects occur with their use. A major disadvantage of these platinum-based anticancer drugs is that resistance can be developed and that they are no longer effective. Therefore, there is a need for the development of new metal-based anticancer drugs. Among these potential new candidates, those based on ruthenium are particularly promising. KP1019 (Indazolium *trans*-[tetrachloridobis (1H-indazole) ruthenate(III)]) (Figure 1) showed promising efficacy in several studies, with fewer side effects than platinum-based anticancer drugs. Further development of this compound led to its sodium salt KP1339 (Sodium *trans*-[tetrachloridobis (1H-indazole) ruthenate(III)]) (Figure 1), which showed a solubility in water. [2]

The mode of action of ruthenium compounds differs from other drugs used in therapy. DNA is not the primary target for ruthenium-based drugs. However, interactions occur with proteins. This fact is also the basis of the fewer side effects. Through intravenous administration, the first potential binding partners include serum proteins (e.g. carrier proteins, immunoglobulin, lipoprotein, enzymes, ..). [3] [4] It was found that the majority of ruthenium (III) compounds are taken up and distributed *in vivo* and *in vitro* via binding to albumin. Likewise, a small proportion of ruthenium-based drugs bind to transferrin. This causes the ruthenium (III) compounds to be transported selectively to the tumour. Tumours have a higher demand for nutrients. Therefore, they also have significantly more receptors for transferrin to cover their increased iron requirement. [1] [2] [3] [5] Effective transport of the metal-based drug is essential for cancer therapy and influences the side effects. The principle of the mode of action of the ruthenium (III) compounds is based on the efficient transport into the tumour and the “activation by reduction” in the tumour tissue. [3] [5] Due to the rapid growth of the tumour, there is an insufficient formation of blood vessels. Consequently, the tumour is not supplied with sufficient oxygen. Together with other numerous factors, this leads to a lower pH value. This environment is ideal for the reduction of Ru(III) to Ru(II) and thus for the activation of the ruthenium-based anticancer drug.

Together with the reduction and the loss of the labile chlorido ligands by hydrolysis, the activation of KP1399 occurs. [1] [6] [7]

It is known from various studies that KP1339 does not bind covalently to albumin after intravenous administration. This non-covalent binding occurs to the hydrophobic sides of the human serum albumin. The non-covalent bond changes into a protein-coordinated one with a longer incubation time. [8] [9] Nevertheless, the actual binding sites are not straightforward to map. Dömötör et al. [8] investigated the preferred binding sites of KP1019 and KP1339 to HSA by a displacement study. These experiments showed that both compounds bind to site I and II of human serum albumin. [8]

The exact mode of action of KP1339 is still not fully understood. But a recent article points out the importance of stress induction on the endoplasmic reticulum. Besides, there is a lower expression of the glucose-regulated GRP78 proteins. [6] Exposure to GPR78 can trigger programmed cell death. Furthermore, resistance to other drugs is reduced. [10]

KP1339 is one of the new auspicious metal-based anticancer drugs. It has shown promising results against neuroendocrine tumours in the clinical trial. KP1339 is mainly effective against tumours, for which platinum-containing anticancer drugs are only partially effective. In some clinical trials, stabilisation of the disease was achieved. [11] [12]

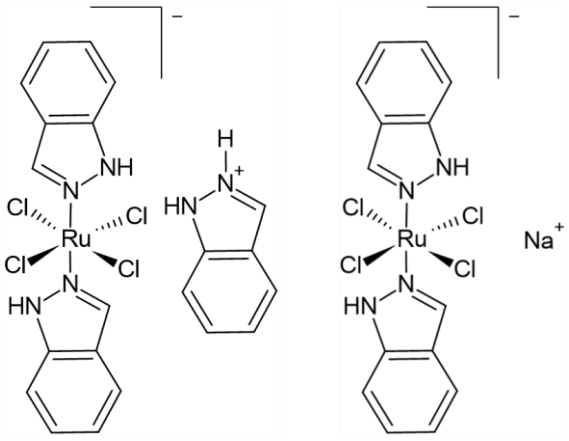

Figure 1: Structure of KP1019 (left) and KP1339 (right) [3]

1.2 ICP-MS

The first inductively coupled mass spectrometer has been launched in the 1980s. Since then it has proven as a powerful tool for multielement analysis to detect trace amounts of the element of interest. In various disciplines it has become the method of choice, for example in environmental, geology and biomedical applications. [13] [14] Due to the multielement capability, different elements can be measured making almost the whole periodic table accessible. Based on a short sample preparation and fast analysis ICP-MS enables a high sample throughput. [15] Further advantages of ICP-MS are the wide linear dynamic range, high sensitivity, good control of interferences, the potential detection of isotopes and the possibility of quantification, even in a complex matrix. [13] [14] [16] The possibility to combine the ICP-MS system with separation techniques such as LC, CE or GC makes it a powerful tool in speciation studies. ICP is a hard ionization technique, where the sample gets completely atomized, which leads to the loss of the structural information during the analysis. Hence, it becomes impossible to detect unknown chemical structures. The combination with other systems like ESI- or MALDI-MS overcomes this drawback. [16]

Aqueous samples get transferred into the gaseous phase by nebulization. [16] Therefore, the samples are transferred directly to the nebulizer through a peristaltic pump or an LC-system. By an incoming argon flow a pneumatic force is generated, this creates a fine aerosol, which is forwarded to the spray chamber. An additional force is required to separate the larger droplets, depending on the spray chamber type it can be a centrifugal (cyclonic) or gravitational (Scott type) force. Usually, the temperature of the spray chamber is set to two degree Celsius, this avoids overloading the plasma and reduces the risk of oxide formation. [15] [17] However, only a small percentage (< 1 %) of the sample gets into the argon plasma, where the sample is dried, vaporized and atomized and single positively charged ions are generated at high temperature (6000-10000 K). Due to the high temperatures, the sample is completely decomposed and the molecular information is lost during this process, that is the reason why only elemental information can be obtained. [17]

The transfer of the ions to the high vacuum area of the mass spectrometer is a critical step. An interface system, which consists of a sample and a skimmer cone, connects the ICP with the MS. Through the cones, the gradual transition from the atmospheric pressure to the high

vacuum pressure is possible. [14] After the ions are passed through the interface, they get guided to the main vacuum chamber by an ion optics system. The ion optics system consists of a series of electrostatic lenses and different designs are available, but the main function is the same. The ion beam gets focused and the background is reduced by removing photons, neutral species, negatively charged ions, which leads to an improved efficiency. The electrostatically focused analytes leave the ion optics in direction of the mass separation device, where the get separated depending on their mass-to-charge ratio. [18]

With ICP there are mainly three different mass analysers (quadrupole, sector field or TOF) combined, whereas the quadrupole analyser is the most frequently used one. The choice of the mass analyser depends on several requirements for instance mass resolution, mass accuracy or data acquisition time. For a long time, a single quadrupole mass analyser was the most frequently used one for multielement analysis. Due to the low resolution an accurate multielement determination was always a challenge. Other techniques were developed to overcome these drawbacks. [19]

A quadrupole mass analyser (Figure 2) consists of four parallel metallic rods, which are arranged in a square (xy-plane). On the two opposite rods the same potential is applied, which is divided into a DC and an AC component. It is possible by changing these two components over time to scan the enter mass range. The ions enter the quadrupole in z-direction and for each m/z ratio there is a specific potential, and this results in a stable trajectory. In case of a unstable trajectory the ion can´t pass and get neutralized at the rods, this leads to a separation based on the mass-to-charge ratio. [15] [20]
The advantages of this device include a high transmission, a high scan speed and a high sensitivity. Furthermore, the quadrupole assembly is low-prized compared to other mass analysers and it easy to handle. [20] A drawback of the quadrupole is that it operates at low resolution (~ 300) therefore it is hardly possible to resolve interferences. [15]

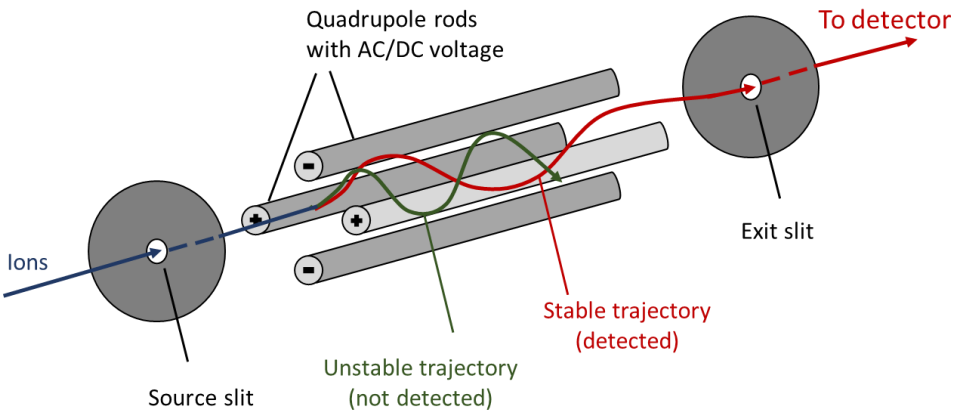

Figure 2: Quadrupole mass analyser [21]

Double focusing sector instruments (Figure 3) consist of a magnetic sector and an electrostatic sector/electrostatic analyser (ESA). In the magnetic sector ions pass through a magnetic field, the field lines a vertical to their direction of movement. An equilibrium arises between Lorentz force and centrifugal force, thus the ions get separated. If the ions have the same speed, then the m/z is the same. The ions, which come from the ion source aren`t monoenergetic and thus ions with a different m/z can have the same impulse. This makes the combination with an electrostatic sector necessary. In the electrostatic sector the ion beam gets focused due to the restriction of the kinetic energy distribution. The arrangement of the magnetic sector and ESA can vary depending on the design of the double focusing sector instrument.

The advantages of this device are the high resolution (~ 7000- 15000) and it enables to resolve interferences. The disadvantages are the high price and the accurate mass measurements are time consuming. [20]

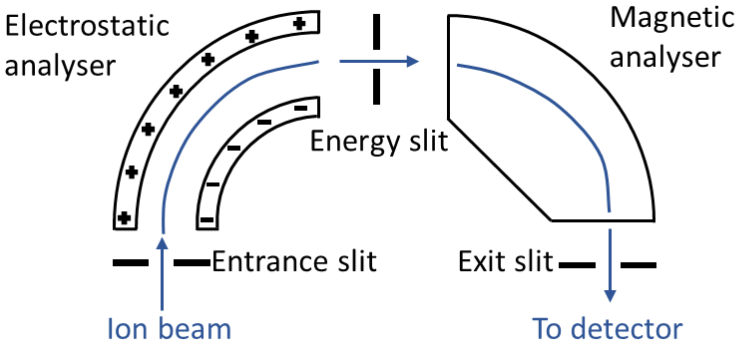

Figure 3: Double focusing sector instrument [22]

The principle of a time-of-flight mass analyser is simple. Ions get accelerated, thereby all get the same kinetic energy. Afterwards they get dispersed in time, depending on m/z, during their flight in a field-free region. Heavier ions arrive later at the detector compared to lighter ones, provided they start at the same time. However, there may be slight differences in the kinetic energy distribution, therefore a TOF is often combined with a reflector/reflectron. The reflector can focus ions with different kinetic energy, this improves the resolution of a TOF analyser. [20]

The advantages of this analyser are the high resolution (~ 10000) and the simultaneous measurement of several m/z. A drawback is the lower sensitivity and the dynamic range. [20] [23]

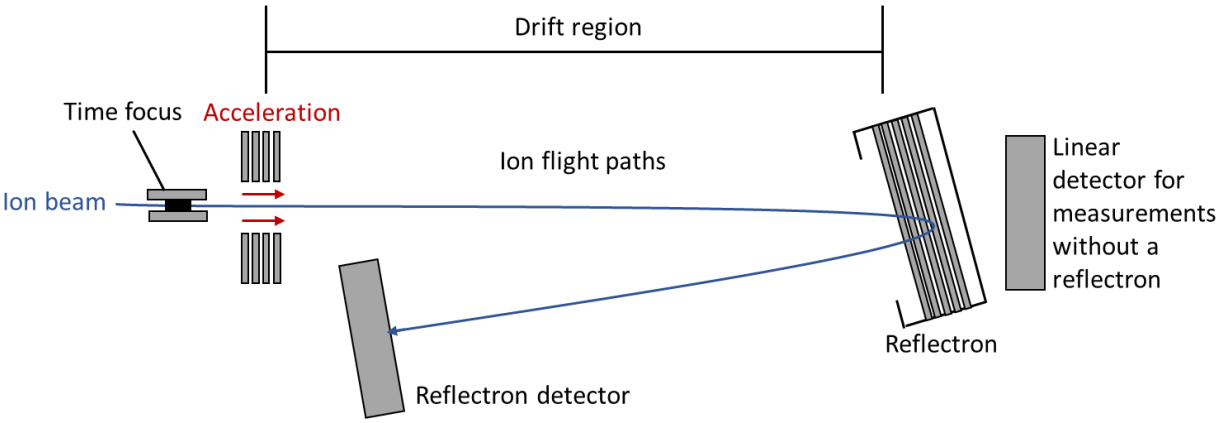

Figure 4: Time-of-flight mass analyser [24]

After the separation of the ions in the mass analyser, they arrive at the detector depending on their mass-to-charge ratio. Typically, a secondary electron multiplier (SEM) is used. It is based at the physical concept of secondary electron emission. When the ions hit the surface of the detector dynode, secondary electrons get released and the signals are processed further by the software. Furthermore, a Faraday cup is used as a detector or in combination with SEM. It is based on the measurement of the ion beam current. It is especially used for an accurate isotope determination. [20] [25]

1.2.1 Tandem mass spectrometry (ICP-MS/MS)

An ICP tandem mass spectrometer has compared to common ICP-CRC (collision/reaction cell) quadrupole mass spectrometer systems an additional quadrupole located in front of the collision/reaction cell (Q1-CRC-Q2) as it is shown in Figure 5, this is the reason why it is often simply referred as a triple quadrupole (ICP-QQQ). This leads to another separation step and the MS/MS setup improves the control over the reaction cell. Consequently, there is an improvement in the selectivity and thus replaces the more expensive and slowly measuring double-focusing sector field devices. Due to the high resolution of the sector field instruments they are normally the method of choice to overcome interferences. In addition, with a higher resolution it is not possible to overcome isobaric interferences and the ion transmission is reduced and thus the sensitivity. The triple quadrupole setup overcomes these drawbacks due to the higher selectivity. [26] [27]

For less challenging applications it is possible to operate the first quadrupole with a wider bandpass, (SQ mode) or it is only used as an ion guide. In the SQ mode the first quadrupole is "fully open" which means that analytes and interferences with the same m/z enter the CRC. This approach is similar to ICP-CRC systems and it is used for less demanding experiments, without a complex matrix or with no present interferences. The mode with a single mass width is termed as MS/MS mode and works with a double mass selection. The first quadrupole acts as a mass filter and thus only selected m/z can reach the collision/reaction cell. Compared to the SQ mode, the ion transmission and thus the sensitivity is reduced in the MS/MS mode. [26] [27]

By using a collision/reaction cell it is possible to avoid interferences (see 1.2.2). Furthermore, reactions and collisions, that are taking place in CRC, can be controlled. This technique can lead to an improvement in the selectivity and efficiency. There are two possible approaches, on-mass and mass-shift. In the case of the on-mass approach, a reactive gas reacts with the interfering ions and thus the analyte can be measured at the original m/z ratio. At the other eventuality, the reaction takes place between the reaction gas and the analyte ion, this leads to a shift of the m/z of the analytes (mass-shift). [26]

In the on-mass approach the same m/z values are selected in both quadrupoles, in contrast to this, in the mass- shift approach different m/z values are selected. In the ICP tandem spectrometry only specific m/z values are selected in the Q1 and all other m/z values get effi-

ciently removed. Thus, no undesired products arise with the reaction gas and interferences and matrix effects are also reduced. [26]

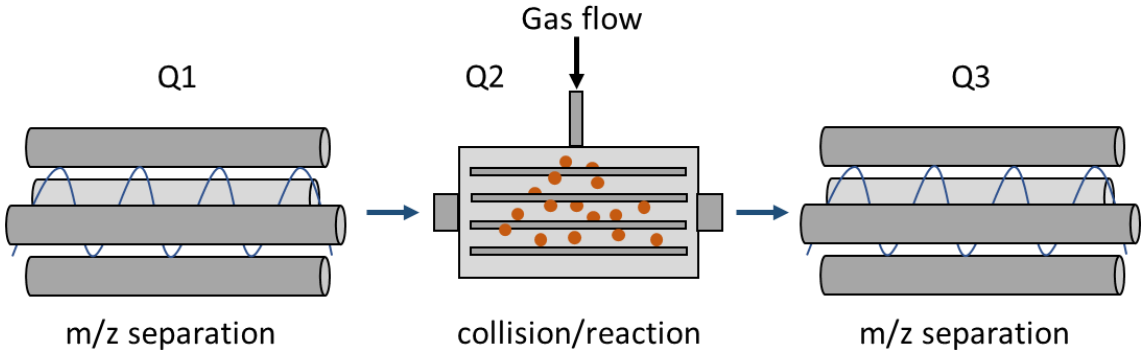

Figure 5: Triple quadrupole setup [28]

1.2.2 Interferences in ICP-MS

Besides the many advantages of ICP-MS, there are also some challenges. Many ICP-devices are coupled with a quadrupole mass analyser. The resolution of this mass analyser is limited to approximately unit resolution. Therefore, it is often not possible to differentiate between analytes and interferences, which have the same mass-to-charge ratio as the analyte. The performance of the ICP-MS can be significantly impaired by these non-spectral and spectral interferences. It is important to be aware of the interferences and eliminate them because they might cause a background and false positives. A well-chosen calibration is essential to eliminate possible non-spectral interferences. The spectral interferences originate from ions with similar mass-to-charge ratio, which compromises the accuracy of the method. To reduce the spectral interferences, it is indispensable to select isotopes with less interferences. [17] [29] [30]

The spectral interferences are divided into isobaric interferences, doubly charged ions and polyatomic ions. [17] [30] Polyatomic interferences are generated by reactions of the sample with the argon plasma, atmospheric gases and compounds of the matrix. [17] [31]

Isobaric interferences are present when ions have a different atomic number but the mass is the same. [14]

Table 1 shows some common spectral interferences in ICP-MS.

Table 1: Spectral interferences in ICP-MS [14] [31]

Type of interference		
Polyatomic interference	$^{52}Cr^{+}$	$^{40}Ar^{12}C^{+}$
	$^{56}Fe^{+}$	$^{40}Ar^{16}O^{+}$
	$^{80}Se^{+}$	$^{40}Ar^{40}Ar^{+}$
	$^{58}Ni^{+}$	$^{40}Ar^{18}O^{+}$
Doubly charged ions	$^{44}Ca^{+}$	$^{88}Sr^{2+}$
	$^{70}Ge^{+}$	$^{140}Ce^{2+}$
	$^{119}Sn^{+}$	$^{238}U^{2+}$
Isobaric Interference	$^{40}Ar^{+}$	$^{40}Ca^{+}$
	$^{54}Fe^{+}$	$^{54}Cr^{+}$
	$^{58}Fe^{+}$	$^{58}Ni^{+}$
	$^{114}Cd^{+}$	$^{114}Sn^{+}$

To prevent interferences, various approaches have been developed in the last few years. On the one hand, it is important to choose the measured isotope carefully, besides mathematical equations can be applied for the correction. Also, the usage of a mass analyser with higher resolution (e.g. TOF, sector field) overcomes interferences. This is limited due to the higher costs of these devices. Most of the ICP-MS devices, which contain a quadrupole mass-analyser, are additionally equipped with a reaction/collision cell (usually an ocotpole). [17] [31] The triple quadrupole ICP-MS is equipped with a reaction/collision cell (octopole). The first quadrupole only conducts ions with a defined mass-to-charge ratio into the octopole, who is located between the first and second quadrupole. After a collision or reaction in the octopole the ion of interest can be detected in the second quadrupole. [32]

In collision cells, there is an inert gas (e.g. Xe, He) used. The interferences are removed by kinetic energy discrimination (KED). Polyatomic species are larger compared to the analyte ions of the same m/z. Therefore, they collide with the collision gas several times on their way through the collision cell and their kinetic energy is reduced. Because of the low kinetic energy these polyatomic ions are excluded from the analysis. However, several analyte ions

get removed, and this is disadvantageous for the sensitivity. Thus, a reaction cell is preferred. [17] [26] [33]

In reaction cells there are specific reaction gases (e.g. O_2, H_2, NH_3) used to remove known interferences by shifting the analyte or the interference to another mass. A critical factor is the selection of the reaction gas. The sensitivity is increased with a reactive gas because the reaction is more efficient. The drawback with a more reactive gas is that there is a higher possibility for additional interferences. The most abundant isotope from sulphur is $^{32}S^+$, which interferes with $^{16}O_2^+$. With O_2 as reaction gas sulphur is efficiently converted into $^{32}S^{16}O^+$ (Figure 6), allowing the measurement from sulphur without interferences. [17] [26] [32]

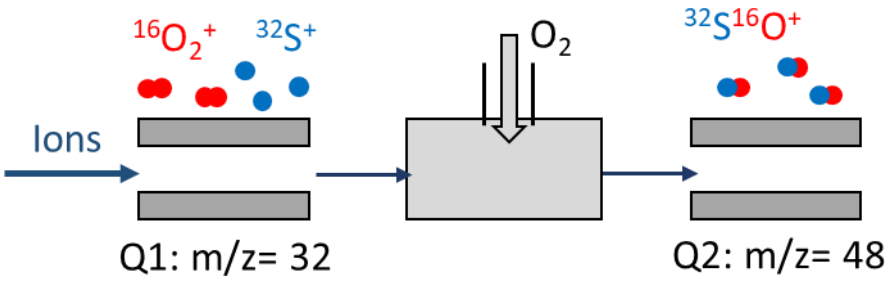

Figure 6: Sulphur measurement in oxygen mode (mass-shift approach) [34]

1.3 ESI-MS

The electrospray ionization is the best-known atmospheric pressure ionization method. ESI is mainly coupled with LC-MS thereby the molecular composition can be investigated. [35]

ESI is a soft ionization method to transfer analytes from the liquid phase to the gas phase gradually to the high vacuum of the mass analyser. This method is especially suitable for large analytes which are non-volatile and easily to charge, for example proteins. Due to the fact, that higher values for the charge (z) compromises the m/z-value, makes high molecular analytes accessible for the analysis in the mass spectrometer. Furthermore, ESI is suitable for metal complexes and other soluble inorganic substances. [20]

The sample solution is guided into a spray capillary and a voltage is applied between this capillary and a counter electrode (transfer capillary). The created electric field induces a charge separation in the liquid and a deformation of the meniscus into a cone (Taylor cone). Fine droplets are emitted from the cone in the direction of the counter electrode. The charge of the droplets depends on the electric field. Due to the Coulomb repulsion, the droplets drift apart, and a fine spray is formed. As the solvent evaporates, the droplet size is

decreasing, and the surface charge density is increasing. To counteract the cooling during the evaporation process, either a heated transfer capillary or a hot nitrogen counterflow is used. As soon as the electrostatic repulsion exceeds the surface tension, the droplets break down into smaller units. The break-up occurs because the Rayleigh limit has been reached. ESI transfers the ions to the mass analyser, which are already present in the solution. Just as well neutral ions are accessible, for example by protonation or deprotonation. [20] [36]
The ions get sampled by a skimmer cone and afterwards they are forwarded to the mass analyser. A quadrupole or an orbitrap are frequently used mass analyser in combination with ESI. [20] [36]

In the following the principals of the orbitrap will be described. The fundamentals of the quadrupole are described in 1.2.

In the orbitrap analyser (Figure 7) the ions are trapped by an electrostatic field. [37] The orbitrap consists of one spindle-shaped central electrode and a two-piece barrel-shaped outer electrode. The central electrode is circled several times to enable an unhindered circling, ultra-high vacuum is required. The ion trajectory is defined by the equilibrium between the centrifugal force and the electrostatic force. The electrostatic force is created by the applying of a voltage. Stable ion trajectories result from the rotation around the central electrode and the axial oscillations. The frequency of the axial oscillation depends on the mass-to-charge ratios. The frequency of the axial oscillation can be detected by using the image current detection. Every m/z value produces a sine wave. The image current signal gets recorded and it is converted into a frequency domain signal with a fast Fourier transformation. [20]
A proper ion injection is essential for this type of mass analyser. The ions are injected into the orbitrap via a curved quadrupole, also known as a C-trap. The ions are accumulated, stored, and thermalized in the C-trap. The C-trap can hold around one million elementary charges. [20]
The orbitrap has proven as a powerful tool for analysis with a high resolution (up to 150 000) and a high mass accuracy. [37]

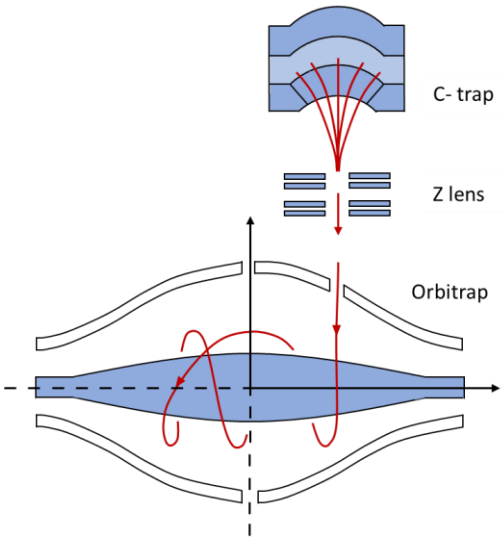

Figure 7: Orbitrap mass analyser [38] [39]

The orbitrap can be combined with other analysers to a so-called hybrid instrument. This allows the advantages of various mass analysers to be combined. The hybrid instruments are mainly used for tandem mass spectrometry. In tandem mass spectrometer, the m/z analysis (MS1) is therefore carried out in the first stage and the ions for the fragmentation are selected. The product ions get selected in a second m/z analyser (MS2) (see 1.2.1). [20]

Despite the possibility to obtain information about the molecular composition that is not possible with ICP-MS, there are still some disadvantages. Ion suppression can occur due to a complex matrix and this has a disadvantageous effect on quantification.[36]

2 Experimental part

2.1 Reagents and materials

The different matrices for the various testing conditions, namely FFBSA, BSA, OA BSA, CoA, FCS, MC0, MC10, and MC10 delipidated were provided by the Medical University of Vienna. For the element analysis, the KP1339 and the solvents to solve the metallodrug (DMSO, 0.9 % NaCl) were kindly provided by the Medical University of Vienna. The Medical University provided the *in vivo* samples of the treated mice (serum samples and blood pellets). The KP1339 for the measurements with organic mass spectrometry was provided from the University of Vienna, Institute of Inorganic Chemistry. For the preparation of the buffer and the dilutions, ultrapure water (18.2 MΩ cm, Milli- Q Advantage) was used.

In Table 2 the details for the used chemicals for the SEC-ICP-MS measurements are given.

The KP1339 and the different matrices were stored in the fridge. The coenzyme A was stored in the freezer at -20 °C and the mice samples were stored at -80 °C.

Table 2: List of used chemicals (SEC-ICP-MS)

Reagent	Purity	Molar mass [g/mol]	Storage conditions	CAS	Hazards	Precautions
HAc	100%, Suprapur	60.05	sufficient ventilation	64-19-7	H226-H314	P210-P280-P301+P330+P331-P303+P361+P353-P305+P351+P338-P310
HNO_3	69%, Suprapur	63.01	sufficient ventilation	7697-37-2	H272-H290-H314-H331	P220-P260-P280-P303+P361+P353-P305+P351+P338-P310
H_2O_2	30%, Suprapur	34.01	sufficient ventilation	7722-84-1	H302-H318-H413	P273-P280-P305+P351+P338-P313
MeOH	≥ 99.9%, for HPLC	32.04	r.t.	67-56-1	H225-H301-H311-H331-H370	P210-P243-P260-P280-P284-P301+P330+P331-P304+P340-P308-P313
NH_3	25%, Suprapur	35.05	sufficient ventilation, cooling	1336-21-6	H314-H335-H400	P273-P280-P301+P330+P331-P305+P351+P338-P308+P310

The performance of the Agilent 8800 ICP-MS-Triple Quadrupole was daily optimized with a tuning solution from Agilent Technologies. The used tune solution (10 µg/L Ce, Co, Li, Tl, Y; Matrix 2 wt% HNO_3) had an end concentration of 1 ppb which required a dilution of 20 mL tune solution with 10 mL HNO_3 and 170 mL ultrapure water.

For the determination of the amount of ruthenium in the blood pellets and the serum samples, the Peak Performance inorganic trace metal standard, ruthenium (Ru), 1000 ± 3 µg/mL in 10 % HCl was used. An internal standard (Indium 100 ppb in 3 % HNO_3) was also used for the determination of ruthenium in the blood pellets.

The following table lists the details from the used chemicals, which were used as mobile phase, for the RP-ESI-MS measurements.

Table 3: List of used chemicals (RP-ESI-MS)

Reagent	Purity	Molar mass [g/mol]	Storage conditions	CAS	Hazards	Precautions
ACN	≥ 99.9%, for LC-MS	41.05	sufficient ventilation	75-05-8	H225-H302+H312+H332-H319	P210-P240-P302+P352-P305+P351+P338-P403+P233
FA	98-100%, Suprapur	46.03	sufficient ventilation	64-18-6	H226-H302-H314-H331	P210-P280-P303+P361+P353-P304+P340+P310-P305+P351+P338-P403+P233
H_2O	MQ= 100 LC- MS grade	18.02	r.t	7732-18-5		

2.2 Sample preparation and instrumentation stability/kinetics measurements

2.2.1 Sample preparation

In the following paragraphs, the steps of the sample preparation are described. All samples, which were measured with the Agilent 8800 ICP-MS/MS were prepared in an ISO class 8 cleanroom to avoid possible contaminations.

2.2.1.1 Preparation stability measurements

For the stability measurements of KP1339 with SEC-ICP-MS, the drug was freshly dissolved in dimethyl sulfoxide (DMSO). Afterwards, the 20 mM stock solution was diluted with 0.9 % sodium chloride (0.9% NaCl). The stability of different drug end concentrations was tested, therefore various dilutions were made and measured repeatedly while being held at 37 °C. In the following table the chosen concentrations are given.

Table 4: Settings for the stability tests of KP1339 (SEC-ICP-MS)

Matrix	KP1339 dissolved in [1)]	End conc. KP1339 [µM]
0.9% NaCl	DMSO	400
		200
		100
		10

[1)] Stock solution KP1339 20mM (dissolved in DMSO)

In addition, the ruthenium content was determined directly after sample preparation (0 h) and after 24 hours with FI-ICP-MS. For the flow injection measurements, KP1339 was dissolved in DMSO and 0.9 % NaCl. The DMSO stock was diluted with PBS, MC0, and 0.9 % NaCl. The NaCl stock solution was only diluted with 0.9 % NaCl.

2.2.1.2 Preparation kinetics measurements

The first settings for the kinetics measurements of the KP1339 DMSO and 0.9 % NaCl stock solution are shown in Table 5. BSA and FFBSA were dissolved in PBS to obtain a concentration of 15.7 g/L, afterwards a ten percent solution was prepared by a second dilution step with PBS. This preparation was in accordance with the cell culture experiments from the Medical University of Vienna. As a ten percent FCS solution was prepared, therefore the FCS stock was diluted with PBS. To compare the effect of a higher FCS concentration, the KP1339 stock solution was diluted with PBS, to obtain a concentration of 200 µM and this solution was diluted one to one with the FCS stock (→ 50 % FCS, FCS 1-1). For the matrices MC0, MC10, and MC10 delipidated, no dilution steps were carried out.

Table 5: Settings for the kinetics measurements of KP1339 (DMSO/0.9% NaCl stock)

KP1339 DMSO stock solution (20mM) [1)]		**KP1339 NaCl stock solution (20mM) [1)]**	
Matrix	**Initial conc. KP1339 [µM]**	**Matrix**	**Initial conc. KP1339 [µM]**
BSA [2)]	400; 200; 100; 10	BSA [2)]	100
FFBSA [2)]	400; 200; 100; 10	FFBSA [2)]	100
MC10	400; 200; 100; 10	MC10	100
MC10 delip.	400; 200; 100; 10	MC10 delip.	100
MC0	100	MC0	100
10% FCS [2)]	100	10% FCS [2)]	100
FCS 1-1 [3)]	100	FCS 1-1 [3)]	100

[1)] Stock solution KP1339 20 mM (dissolved in DMSO or 0.9 % NaCl)

[2)] BSA, FFBSA, FCS stock solutions were diluted with PBS → 10 % solution

[3)] Stock solution was diluted with PBS → 200µM, afterwards 1:1 dilution with FCS (50% FCS)

The measurements for the KP1339 0.9 % NaCl stock solution (Table 5) were carried out after the measurements for the DMSO stock solution. The first measurements showed that the 100 µM initial concentration provides sufficient intensities. Thus, only one concentration was measured in all other settings.

The KP1339 DMSO stock solution was also tested with additional CoA. The CoA was stored at -20 °C and was freshly dissolved in ultrapure water to obtain a 20 mM stock solution. After-

wards 100 µM CoA was added to MC10, MC0, and PBS. In the following Table the conditions for the measurements with CoA are shown.

Table 6: Settings for the kinetics measurements of KP1339 (DMSO stock) with CoA

KP1339 DMSO stock solution (20mM) [1)]		
Matrix	**Initial conc. KP1339 [µM]**	**Initial conc. CoA [2)] [µM]**
MC10	100	100
MC0	100	100
PBS	100	100

[1)] Stock solution KP1339 20 mM (dissolved in DMSO)

[2)] Stock solution CoA 20 mM (dissolved in H_2O)

Another set of test conditions included matrices that were spiked with BSA, FFBSA, or OA BSA. Therefore, BSA, FFBSA, and OA BSA were dissolved/diluted in PBS (c_{SET}= 15.7 g/L), and afterwards a ten percent solution with MC0, or PBS was prepared. The settings for the KP1339 and 0.9 % NaCl stock solution are listed in Table 7.

Table 7: Settings for the kinetics measurements of KP1339 (DMSO/0.9% NaCl stock) in spiked matrix

KP1339 DMSO stock solution (20mM) [1)]		**KP1339 NaCl stock solution (20mM) [1)]**	
Matrix	**Initial conc. KP1339 [µM]**	**Matrix**	**Initial conc. KP1339 [µM]**
MC0 + BSA [2)]	100	MC0 + BSA [2)]	100
MC0 + FFBSA [2)]	100	MC0 + FFBSA [2)]	100
MC0 + OA BSA [2)]	100	MC0 + OA BSA [2)]	100
PBS + OA BSA [2)]	100	PBS + OA BSA [2)]	100

[1)] Stock solution KP1339 20 mM (dissolved in DMSO or 0.9 % NaCl)

[2)] BSA, FFBSA, OA-BSA were diluted/dissolved in PBS, afterwards dilution with MC0 or PBS → 10% solution

2.2.2 Instrumental parameters

For the stability and kinetics measurements of KP1339, an Agilent 8800 ICP-MS Triple Quadrupole (Agilent Technologies, Tokyo, Japan), equipped with a collision/reaction cell was used. For chromatographic separation, an Agilent 1260 Infinity Bio-Inert LC system (Agilent Technologies, Waldbronn, Germany) was coupled via a PEEK tubing directly to the nebulizer of the ICP-MS/MS. For the measurement and evaluation of the samples, the ICP-MS system was operated with the MassHunter 4.5 Software Package (Version C.01.05 2018). The experimental parameters are listed in Table 8 and Table 9.

All measurements, which were performed with the Agilent 8800 ICP-MS were done in an ISO class 7 cleanroom, to reduce possible contaminations.

Oxygen was selected as reaction gas for the ICP-MS/MS measurements. Therefore, sulphur was monitored as $^{32}S^{16}O^{+}$. For the separation, a size-exclusion chromatography was performed. The final separation for the kinetics measurement was carried out with an Acquity UPLC Protein BEH SEC Column (1.7 µm, 4.6 x 150 mm, 10-450 K) from Waters. For the stability measurements, also a column from Waters was used, but with a different pore size (125 Å). With the 200 Å column a faster separation (20 minutes per measurement, 30 minutes for + CoA measurements) was possible. Ammonium acetate (50 mM, pH 6.8) was used as mobile phase. For the kinetics and stability tests, different time points were chosen, while the samples were being held at 37 °C.

Table 8: Instrumental parameters of the ICP- MS/MS system

RF power	1550 V
Sampling depth	7.8 mm
Spray chamber	quartz, double pass
Spraying chamber temperature	2 °C
Plasma gas	15 L/min
Auxiliary gas	0.9 L/min
Nebulizer gas	1.07 L/min
Reaction gas	0.3 mL/min O_2
Cones	Ni
Cell Entrace	-100 V
Cell Exit	-60 V
Integration time	0.1s
Mode	TRA
Measured isotopes	^{32}S, ^{101}Ru, ^{102}Ru
Measured masses	48, 101, 102

Table 9: Instrumental parameters of the HPLC- system

Column	Waters Acquity UPLC Protein BEH SEC
Material	BEH
Separation type	Size exclusion
Pore size	200 Å [1)] / 125 Å [2)]
Particle size	1.7 µm
Inner diameter	4.6 mm
Length	150 mm
Mass range 125 Å	1K - 80K Daltons
Mass range 200 Å	10K - 450K Daltons
Eluents	50 mM NH_4Ac, pH 6.8
Injection volume	5 µL
Flow rate	0.4 mL/min
Column temperature	37 °C
Autosampler temperature	37 °C [1) & 2)] / 4°C [3)]
Run time	20 min [1)] / 30 min [2)]

[1)] kinetics measurements

[2)] stability measurements

[3)] serum: binding and determination c_{Ru}

For the investigation of the possible decrease of the ruthenium content in different settings over time, flow injection was employed using the Agilent 1260 Infinity Bio-Inert LC system in combination with the Agilent 8800 ICP-MS/MS. Therefore, the samples were measured directly after sample preparation (0 h) and after 24 hours. The instrumental parameters were the same as in Table 8 and Table 9.With the exception that the autosampler temperature has been lowered to 4 °C and only the two ruthenium isotopes were measured.

2.3 Determination of the Ru concentration in blood pellets of mice treated with KP1339 or KP1339/etomoxir

In the following, the steps of the sample preparation and the instrumental parameters for the determination of the ruthenium concentration in the mice blood pellets are described. All samples were measured with the Agilent 7800 ICP-MS. The standards were produced gravimetrically.

2.3.1 Sample preparation

A part of the blood pellet (10- 30 mg) was weighed in a PFA vessel. Afterwards, 2 mL 20 % HNO_3 and 100 µL H_2O_2 were added. The heating program for the open vessel digestion was six hours long (Figure 8). The absolute time can vary because the next step was applied when the temperature of the previous step has been reached. After the digestion procedure, the PFA vessels were cooled off. Each sample was transferred to a 15 mL falcon tube and the PFA vessel was rinsed two times with 4 mL ultrapure H_2O and transferred to the tube. The dilution factor was obtained by dividing output weight by initial weight. The same procedure was followed for the blanks. After that, the samples were measured with the 7800 ICP-MS from Agilent (2.3.2 Instrumental parameters).

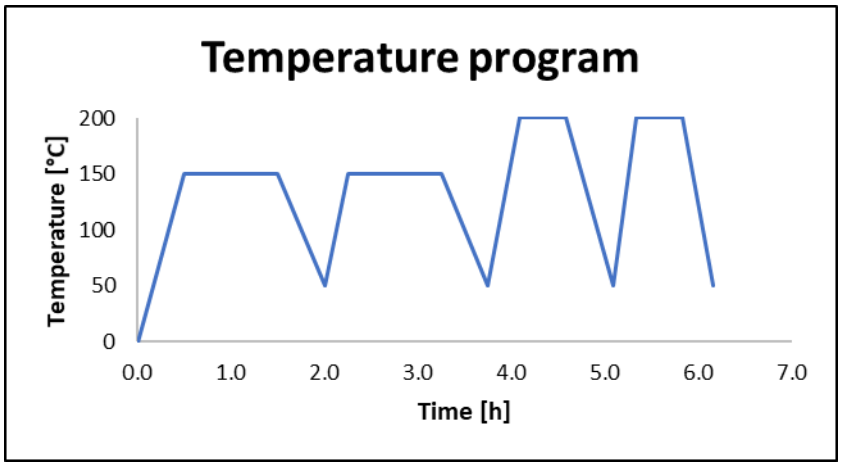

Figure 8: Temperature program open vessel digestion

2.3.2 Instrumental parameters

The digested blood pellets were measured in direct infusion with an Agilent 7800 ICP-MS Single Quadrupole system (Agilent Technologies, Tokyo, Japan). The measurement was operated with the MassHunter 4.4 software package (Version C.01.04). Indium was measured as an internal standard. The experimental settings are given in Table 10.

Table 10: Instrumental parameters direct infusion ICP-MS

Direct infusion	
Instrumental parameters for the 7800 ICP-MS device	
Autosampler	Agilent SPS 4
RF power	1550
Plasma gas	15 L/min
Auxiliary gas	0.9 L/min
Nebulizer gas	1.07 L/min
Cones	Ni
Integration time	0.1 s
Mode	no gas
Measured isotopes	^{101}Ru, ^{102}Ru, ^{115}In
Measured masses	101, 102, 115
Number of replicates	10
Number of sweeps	100

2.4 Investigation of serum samples of mice treated with KP1339 or KP1339/etomoxir

In the following paragraphs the sample preparation and the instrumental parameters for the measurements of the mice serum samples are described. In the serum samples, the ruthenium concentration was determined on the one hand, but the protein binding was also examined. All samples, which were measured with the Agilent 8800 ICP-MS/MS were prepared in an ISO class 8 cleanroom to avoid possible contaminations. All standards were produced gravimetrically.

2.4.1 Sample preparation

To investigate the binding of KP1339 to serum proteins *in vivo*, the serum samples of mice treated with KP1339 and KP1339/etomoxir were analysed by SEC-ICP-MS using the instrumental parameters described in 2.4.2. For this purpose, mouse serum samples were diluted appropriately in 50 mM NH_4Ac buffer (pH 6.8) directly before the measurement.

Flow injection in combination with ICP-MS/MS detection was used to determine the ruthenium concentrations directly in mouse serum samples. Serum samples were diluted in 50 mM NH_4Ac buffer (pH 6.8) to match the calibration range of the standards. Standards were prepared in 3 % HNO_3. Diluted serum samples were kept at 4 °C in the autosampler of the HPLC-system.

2.4.2 Instrumental parameters

The protein binding of KP1339 and the amount of ruthenium in mouse serum was also investigated with the 8800 ICP-MS/MS system from Agilent. For both test series the HPLC-system was coupled to the ICP-MS. The settings for the protein binding study are the same as in Table 8 and Table 9. With the exception that the autosampler temperature for the determination of the protein binding was set to 4 °C. For the investigation of the protein binding, the Acquity UPLC Protein BEH SEC Column (1.7 µm, 4.6 x 150 mm, 10-450 K) from Waters was used. For the investigation of the protein binding, the ruthenium isotopes and sulphur were registered. For the investigation of protein binding, all serum samples were measured once. For the determination of the total ruthenium amount no column was needed, a flow injection was carried out. The settings for the flow injection of the mice serum samples are listed

in Table 11 and Table 12. Since no sulphur was measured in this measurement, no reaction gas was used.

Table 11: Instrumental parameters ICP-MS/MS; flow injection

RF power	1550 V
Sampling depth	8.0 mm
Spray chamber	quartz, double pass
Spraying chamber temperature	2 °C
Plasma gas	15 L/min
Auxiliary gas	0.9 L/min
Nebulizer gas	1.07 L/min
Reaction gas	/
Cones	Ni
Cell Entrace	-40 V
Cell Exit	-50 V
Integration time	0.1 s
Total Acquisition Time	0.5 min
Mode	TRA
Measured isotopes	^{101}Ru, ^{102}Ru
Measured masses	101, 102

Table 12: Instrumental parameters HPLC-system; flow injection

Eluents	50 mM NH_4Ac, pH 6.8
Injection volume	2 µL
Flow rate	0.4 mL/min
Autosampler temperature	4 °C

2.5 Sample preparation and instrumentation RP-ESI-MS measurements

2.5.1 Sample preparation

In the following paragraphs, the steps of the sample preparation for the stability and kinetics measurements with organic mass spectrometry are described.

2.5.1.1 Preparation stability measurements

For the stability measurements with RP-ESI-MS KP1339 was dissolved in 0.9 % NaCl to obtain a 20 mM stock solution. For the comparison of the stability of the compound, one approach was dissolved in the ultrasonic bath, and the other one was dissolved by vortexing. The stock solutions were diluted with 0.9 % NaCl to obtain a 400 µM end concentration. To investigate the influence of the pH value, the pH value for one sample was adjusted to three using 0.1 M HCl. In the following table, all details are shown.

Table 13: Settings for the stability measurements with RP-ESI-MS in 0.9% NaCl

KP1339 NaCl stock solution [1)]					
Matrix	**V_{Matrix} [µL]**	**$V_{KP1339\ stock}$ [µL]**	**KP1339 dissolved in**	**Solved by**	**End conc. KP1339 [µM]**
0.9% NaCl	980	20[1)]	0.9% NaCl	Ultrasonic bath	400
	980	20[1)]		Vortexing (pH ~7)	400
	980	20[1)]		Vortexing (pH ~3)	400

[1)] Stock solution KP1339 20mM (dissolved in 0.9% NaCl)

An aliquot was taken from the prepared sample and stored at 4 degree Celsius. The first measurement was taken directly after sample preparation. After 24 hours, the samples were measured, which were stored at 37 °C for 24 hours. In addition, the cooled aliquot was measured. Thus, the influence of the temperature on the stability could be investigated.

2.5.1.2 Preparation kinetics measurements

For the measurements with RP-ESI-MS KP1339 was freshly dissolved in DMSO to obtain a 20 mM stock solution. For the dissolving step, it was necessary to vortex briefly. Then the stock was diluted with MC0 and the initial concentration of KP1339 was 400 µM. An attempt was made to dissolve KP1339 in MC0. In addition to vortexing, the stock solution was placed in an ultrasonic bath, and the stock solution was spun because the KP1339 wasn´t completely soluble in MC0. Afterwards the 10 mM stock solution was diluted with MC0 to obtain a 400 µM initial concentration of KP1339. Furthermore, samples were prepared with MC10. For these measurements, KP1339 was dissolved in DMSO. Afterwards, the stock solution was diluted with MC10 to obtain the desired initial concentration of 400 µM.
In Table 14 the test settings for the kinetics measurements are listed.

Table 14: Settings for the kinetics measurements with RP-ESI-MS in MC0 and MC10

KP1339 stock solution		
Matrix	**KP1339 dissolved in**	**Initial conc. KP1339 [µM]**
MC0	DMSO	400
	MC0	400
MC10	DMSO	400

2.5.2 Instrumental parameters

For the structural elucidation of KP1339 in medium, an LTQ Orbitrap Velos (Thermo Fisher) was used. For the chromatographic separation the instrument was coupled to the Thermo Fisher Vanquish UHPLC-system. The LC-system was run with the Chromeleon software (Version 7.2.6) and the Velos was operated with the Thermo Xcalibur 2.2 SP 1.48 (2011).
The instrumental parameters for the RP-ESI-MS measurements are summarized in Table 15.

Table 15: Instrumental parameters RP-ESI-MS

Instrumental parameters for the LTQ Orbitrap Velos	
Resolution MS1	60 000
Resolution MS2	15 000
Scan ranges	140.00 - 1500.00 m/z
Polarity	Positive/Negative
Dynamic exclusion	
Exclusion duration	2 s
Scan event	
Minimum signal threshold	15 000 counts
Analyse top N peaks	3
Activation type	CID
Isolation width	3 m/z / 16 m/z
Normalised collision energy	35.0
Activation time	30.0 ms
Instrumental parameters for the HPLC-system	
Column	Thermo Fisher Acclaim™ 120 C18 3µm
Material	Dionex Bonded Silica Products
Seperation type	Reversed phase
Pore size	120 Å
Inner diameter	2.1 mm
Length	150 mm
Eluents	ACN/H_2O + 0.1 % FA
Injection volume	10 µL
Flow rate	0.45 mL/min
Column temperature	25 °C
Autosampler temperature	37 °C
Run time	60 min

A gradient of acetonitrile + 0.1 % formic acid and water + 0.1 % formic acid was used as mobile phase. The run time for each measurement was sixty minutes. In Table 16 the exact composition of the gradient is given and in Figure 9 it is graphically represented.

Table 16: Flow gradient Vanquish UHPLC

No.	Time [min]	Flow [mL/min]	ACN + 0.1 FA % [%]	H_2O + 0.1 FA [%]
1	0.00	0.45	5.0	95.0
2	45.00	0.45	95.0	5.0
3	51.50	0.45	95.0	5.0
4	52.00	0.45	5.0	95.0
5	59.00	0.45	5.0	95.0

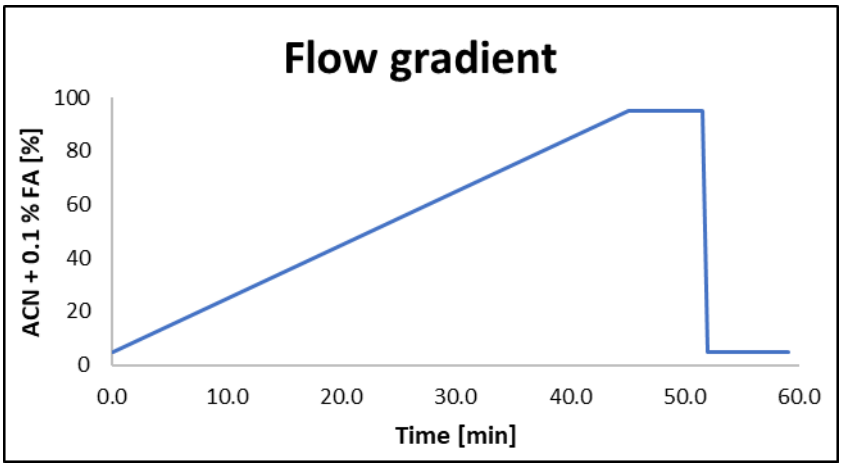

Figure 9: Flow gradient Vanquish UHPLC

For the stability measurements, almost the same method as in Table 15 was used. The only exceptions were that the injection volume was 5 µL instead of 10 µL, and the samples were only measured in negative mode. Furthermore, an additional measurement was carried out at 4 °C.

3 Results and discussion

3.1 ICP-MS

Due to the high sensitivity, ICP-MS was the method of choice for the stability and kinetics measurements of the ruthenium-based anticancer compound KP1339. Besides, the wide dynamic range it is advantageous for the determination of the ruthenium content. The determination of sulphur is not straightforward because the most abundant sulphur isotope (^{32}S, abundance 95.02%) interferes with the $^{16}O_2^+$ ion. By using a triple quadrupole, even sulphur can be detected. In this work, such a device was used and, using oxygen as a reaction gas, sulphur could be detected as $^{32}S^{16}O^+$. These problems do not occur with ruthenium, the isotopes can be determined with a single quadrupole.

3.1.1 Stability measurements

The selection of the medium to dissolve a compound is crucial to ensure that the compound remains in its intact form before the start of *in vitro* studies. Therefore, the stability of KP1339 was investigated in different media, which are commonly used in cell culture experiments. In a first experiment, the stability of KP1339 was investigated in 0.9 % NaCl dilutions from a DMSO KP1339 stock solution by SEC-ICP-MS/MS measurements. In another setting, the ruthenium content was determined with FI-ICP-MS. Therefore, the KP1339 DMSO stock solution was diluted with MC0, PBS, and 0.9 % NaCl. The stability of the 0.9 % NaCl stock solution, which was further diluted with 0.9 % NaCl, was also investigated.

For the stability measurements of KP1339 by SEC-ICP-MS/MS, the samples were injected several times over 24 hours while being held at 37 °C. The separation by size-exclusion chromatography enabled to track KP1339 via its ruthenium trace over time and to follow the stability in the respective end concentration.

The dilution of KP1339 in 0.9 % NaCl from a highly concentrated stock solution of KP1339 in DMSO was not stable over time. At higher concentrations (200 µM and 400 µM) precipitation could be observed in the HPLC vial. The following Figure shows the decrease of the ruthenium area over time.

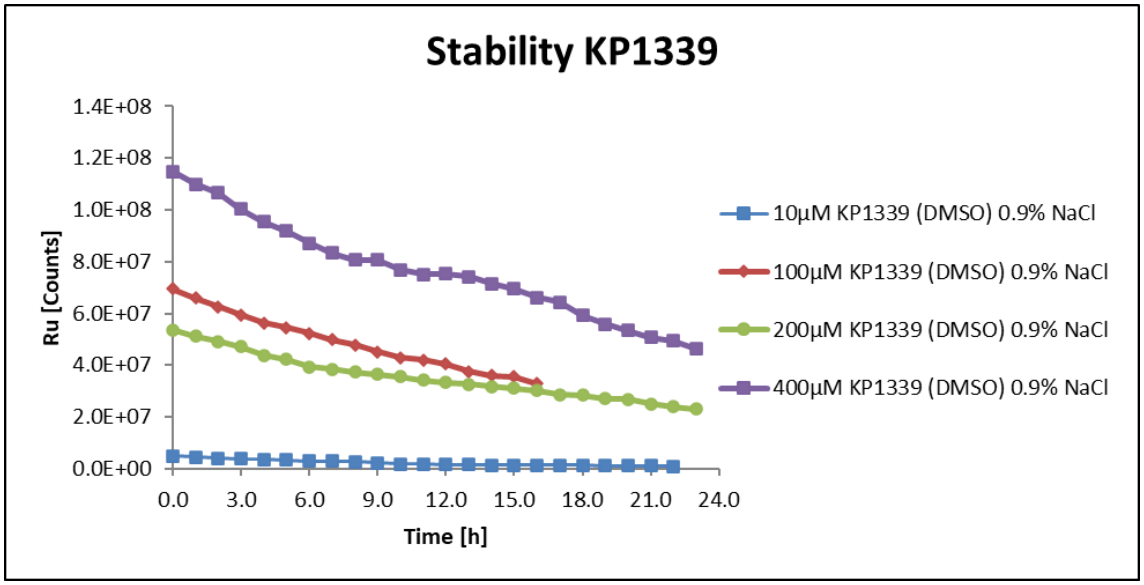

Figure 10: Stability of KP1339 (DMSO) in 0.9% NaCl, SEC- ICP- MS

The following Table lists the percentage decrease of the ruthenium counts of the KP1339 DMSO stock solution, which was diluted with 0.9 % NaCl over a time period of 16 and 23 hours respectively (See Figure 10). The highest decrease of Ru counts was observed for the solution with the lowest end concentration. Based on the observed precipitation, this would rather have been expected for the higher end concentrations.

Table 17: Change ruthenium counts in the KP1339 DMSO stock solution (SEC-ICP-MS)

KP1339 DMSO stock solution [1)]		
Matrix	**End conc. KP1339 [µM]**	**Decrease Ru counts [%]**
0.9% NaCl	400	59.6
	200	57.1
	100	52.8
	10	79.1

[1)] Stock solution KP1339 20 mM (dissolved in DMSO)

In addition, the ruthenium content was determined directly after sample preparation (0 h) and after 24 hours with FI-ICP-MS. The KP1339 DMSO stock solution was stable in MC0 for at least 24 hours. In all other settings, a decrease of the ruthenium content was observed. The results for both stock solutions are summarized in Table 18.

Table 18: Change of ruthenium counts in the KP1339 DMSO and 0.9% NaCl stock solution (FI-ICP-MS)

KP1339 DMSO stock solution [1]		KP1339 0.9% NaCl stock solution [2]	
Matrix	**Decrease Ru counts [%]**	**Matrix**	**Decrease Ru counts [%]**
MC0	no decrease	0.9% NaCl	70.1
PBS	26.6		
0.9% NaCl	78.6		

[1] KP1339 dissolved in DMSO

[2] KP1339 dissolved in 0.9% NaCl

Due to the decrease of the ruthenium counts over time and thus the lack of stability in various media (PBS, 0.9 % NaCl), all solutions should always be freshly prepared.

3.1.2 Kinetics measurements of KP1339 in different biological matrices

Numerous experiments in cell culture have led to several hypotheses. These should be investigated in further methods.

To examine the behavior of KP1339 and investigate the protein binding kinetics in different biological matrices, SEC-ICP-MS measurements were carried out. The samples were injected several times over a period of 24 hours, depending on the biological matrix, while being held at 37 °C in the autosampler of the HPLC-system. The separation with the used size-exclusion column enabled to follow the binding of KP1339 to albumin.

In Figure 11, the sulphur peaks corresponding to albumin (66.5 kDa [40], retention time of around 4 min) and its dimer (retention time of 3.5 min) and the ruthenium peak corresponding to intact KP1339 (retention time of 15 min) are shown. The chromatograms are from a KP1339 DMSO stock solution in BSA and was measured directly after sample preparation (time point 0 h). For the kinetics measurements by SEC-ICP-MS, an analysis time of approximately 20 minutes per sample was chosen. After 24 hours, the binding of KP1339 to albumin and its dimer is evident, whereas no free KP1339 can be detected any more (Figure 12).

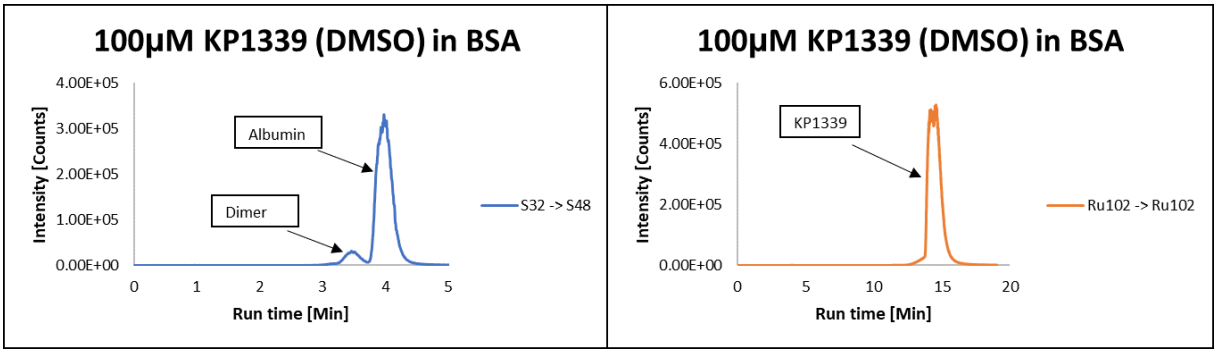

Figure 11: Albumin and KP1339 peak of 100µM KP1339 (DMSO) in BSA_0h

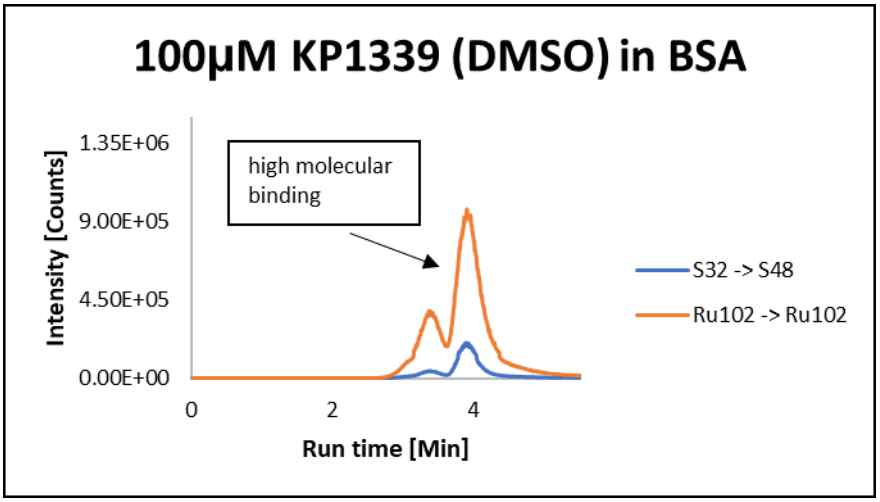

Figure 12: Albumin and KP1339 peak of 100µM KP1339 (DMSO) in BSA_24h

3.1.2.1 Kinetics measurements in BSA/FFBSA/MC10/MC10 delipidated

In a next step, the protein binding kinetics of KP1339 from two different stock solutions (one in DMSO and one in 0.9 % NaCl) were investigated in different biological matrices using SEC-ICP-MS. Thus, on the one hand the influence of the solvent but also the role of the medium could be investigated. For this purpose, bovine serum albumin (the most abundant protein in serum) and fat free BSA were selected, as it was shown in cell culture experiments that KP1339 showed lower cytotoxicity at a higher fat content. Thus, the question arose if the fat content of the medium influences the uptake into the cell. The results of the cell culture experiments led to the hypothesis that KP1339 could bind to a fatty acid and this in turn influences the binding to albumin. In addition to BSA/FFBSA, also MC10 (cell culture medium with 10% fetal calf serum) and M10delip. were included.

The following Figures (Figure 13 to Figure 16) show the decrease of KP1339 (diluted from a DMSO stock solution) over time as a function of the initial concentration in different biologi-

cal settings. It can be seen that the protein binding kinetics is significantly faster at lower KP1339 initial concentrations in all 4 media. KP1339 binds faster to albumin in MC10, and MC10delip. compared to BSA, and FFBSA. FCS added to the medium is significantly more complex than pure BSA/FFBSA. Likewise, the albumin and fatty acid content can vary significantly. This fact and the numerous other components in McCoy`s 5A Medium (see 5 Appendix) can thus possibly have an influence on the protein binding kinetics. In BSA and FFBSA (Figure 13 and Figure 14), the percentage decrease in KP1339 was comparable over time. These measurements therefore did not confirm the assumption that fat could influence the protein binding to a large extent.

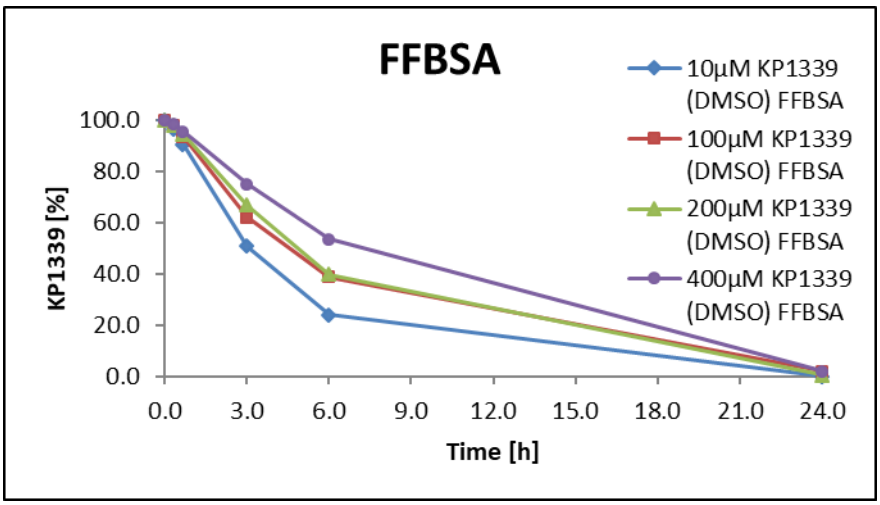

Figure 13: Kinetics measurements of different KP1339 initial conc. (DMSO stock solution) in FFBSA

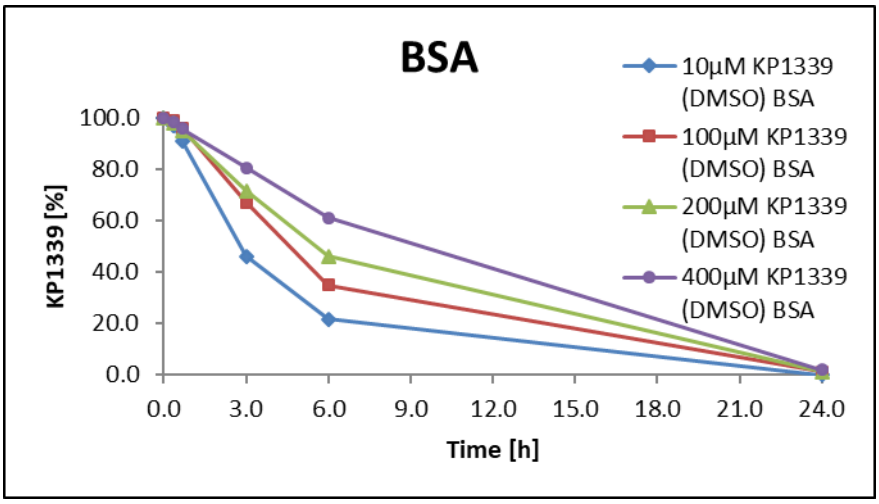

Figure 14: Kinetics measurements of different KP1339 initial conc. (DMSO stock solution) in BSA

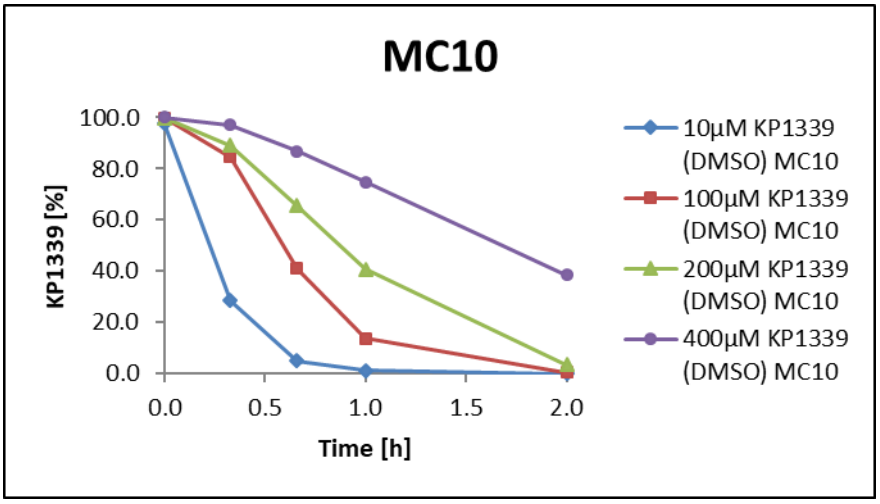

Figure 15: Kinetics measurements of different KP1339 initial conc. (DMSO stock solution) in MC10

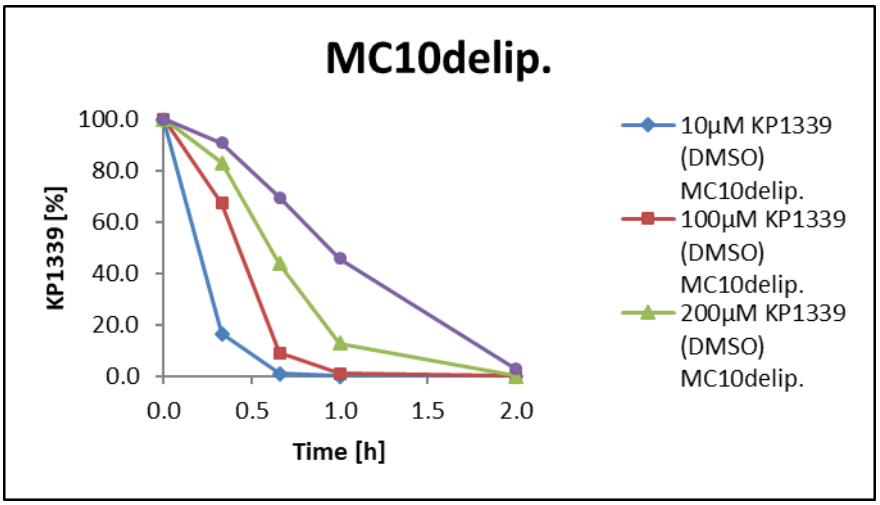

Figure 16: Kinetics measurements of different KP1339 initial conc. (DMSO stock solution) in MC10delip.

In Figure 17, the protein binding kinetics of the KP1339 NaCl stock solution in FFBSA, BSA, MC10, and MC10delip. are shown. The kinetics are clearly faster in the 0.9 % NaCl stock solution compared to the DMSO stock solution (Figure 13 to Figure 16).

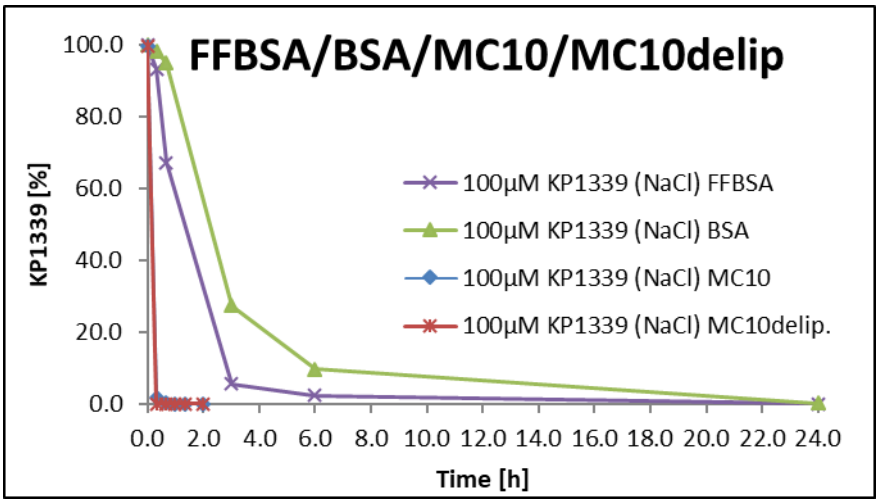

Figure 17: Kinetics measurement of KP1339 (NaCl stock solution) in FFBSA/BSA/MC10/MC10delip.

The following Table (Table 19) shows the decrease of the KP1339 0.9 % NaCl and DMSO stock solution in FFBSA, BSA, MC10, and MC10 delipidated. By comparing the percentage decrease it becomes more obvious that the kinetics are significantly faster for KP1339, which was dissolved in 0.9 % NaCl. In many cell cultures experiments for KP1339, DMSO is used as a solvent, whereas in the *in vivo* experiments 0.9 % NaCl is used. But as these results show that there are significant differences in the protein binding kinetics of KP1339, this fact has to be considered for the interpretation of results.

Table 19: Decrease of 100µM KP1339 (DMSO and NaCl stock) in FFBSA/BSA/MC10/MC10delip. over time

		KP1339 DMSO stock solution [1]	KP1339 NaCl stock solution [2]
Matrix	**Time [h]**	**KP1339 [%] [3]**	**KP1339 [%] [3]**
FFBSA	0.00	99.95	99.93
	0.33	97.94	93.29
	0.66	93.60	67.31
	3.00	62.14	5.53
	6.00	38.81	2.29
	24.00	2.13	0.11
BSA	0.00	99.94	99.95
	0.33	98.89	98.36
	0.66	96.26	95.01
	3.00	67.10	27.41
	6.00	35.00	9.67
	24.00	1.12	0.14
MC10	0.00	99.77	99.87
	0.33	84.61	1.86
	0.66	40.94	0.15
	1.00	13.71	0.00
	1.33	/	0.00
	2.00	0.40	0.00
MC10 delip.	0.00	99.90	99.78
	0.33	67.29	0.00
	0.66	9.03	0.00
	1.00	0.95	0.00
	1.33	0.00	0.00
	2.00	0.00	0.00

[1] Stock solution KP1339 20 mM (dissolved in DMSO)

[2] Stock solution 20mM (dissolved in 0.9% NaCl)

[3] End conc. KP1339 in Matrix → 100µM

3.1.2.2 Kinetics measurements in FCS

In Figure 18, the kinetics of the KP1339 0.9 % NaCl and DMSO stock solution as a function of the serum concentration is compared. Due to the measurement in different FCS concentrations, the albumin content also varies. Thus, the dose dependence of the protein binding was investigated.

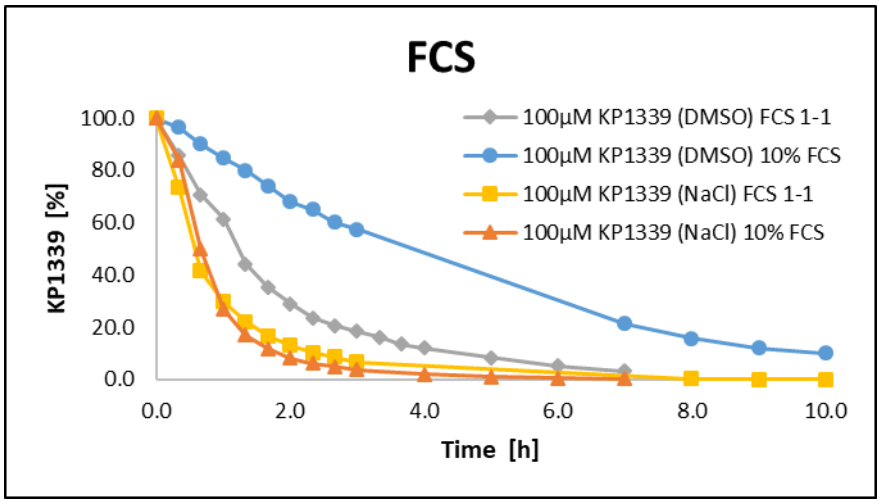

Figure 18: Kinetics measurements KP1339 DMSO and NaCl stock solution in FCS

The protein binding kinetics of the 0.9 % NaCl dissolved KP1339 is hardly affected by the different FCS concentrations. On the other hand, KP1339, which was dissolved in DMSO, binds significantly faster if more serum, and thus a higher albumin content, is present

In FCS it is again clearly recognisable that the kinetics in the KP1339 0.9 % NaCl stock solution are significantly faster compared to the KP1339 DMSO stock solution.

3.1.2.3 Kinetics measurements in MC0

In a next experiment, the protein binding kinetics of KP1339 were investigated in cell culture medium without the addition of FCS (M0). In both stock solutions (DMSO and 0.9 % NaCl), the absence of serum proteins and especially albumin revealed other possible binding partners for KP1339. The peak corresponding to the intact form of KP1339 disappeared over time and ruthenium was detected in the low-molecular weight fraction, where several Ru containing substances were observed. The Ru species can be either degradation products of KP1339 and/or KP1339 and its degradation products bound to small molecular substances present in M0.

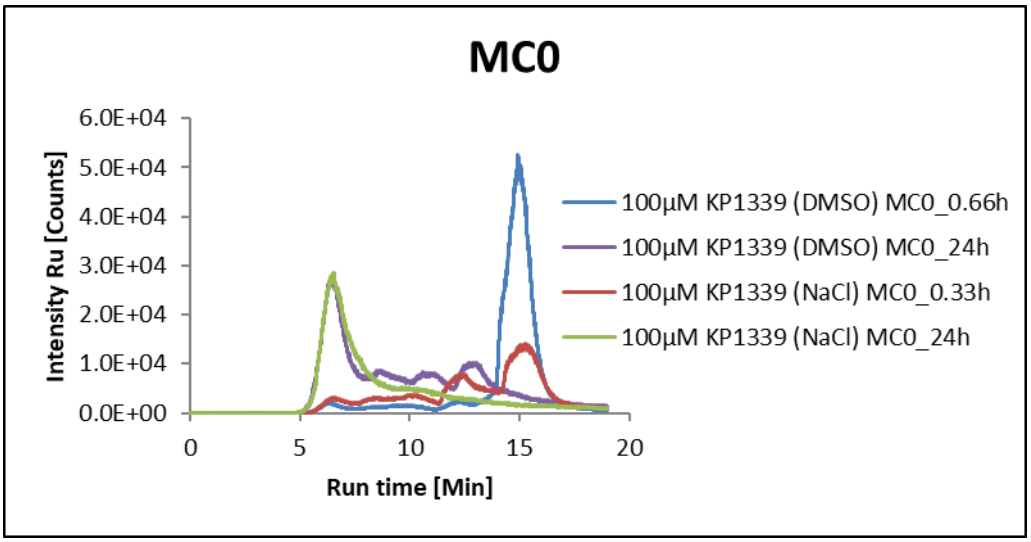

Figure 19: Chromatogram KP1339 DMSO and NaCl stock solution in MC0

3.1.2.4 Kinetics measurements with additional CoA

CoA forms with etomoxir a thioester. By adding CoA to KP1339 and PBS, MC0, and MC10, it should be investigated whether a thioester is also formed with KP1339. Or whether there is an influence due to the addition of CoA on the binding kinetics of KP1339. The addition of CoA led to a shift in the retention time of KP1339. Therefore, the run time was increased to 30 minutes instead of 20 minutes.

The comparison of the KP1339 0.9 % NaCl stock solution and the DMSO stock solution with/without CoA in MC10 is shown in Figure 20. By comparing the KP1339 (DMSO) in MC10 and the sample with the additional CoA, it is evident that the protein binding is accelerated by the addition of CoA. After the addition of 100 µM CoA, no free KP1339 can be observed any more after 0.5 h. The binding of the KP1339 0.9 % NaCl stock solution in MC10 takes also place very quickly and after 20 minutes hardly any free KP1339 is left. As for MC10, the binding of KP1339 to albumin was accelerated by the addition of CoA, this method or medium is not suitable for investigating whether a thioester is formed.

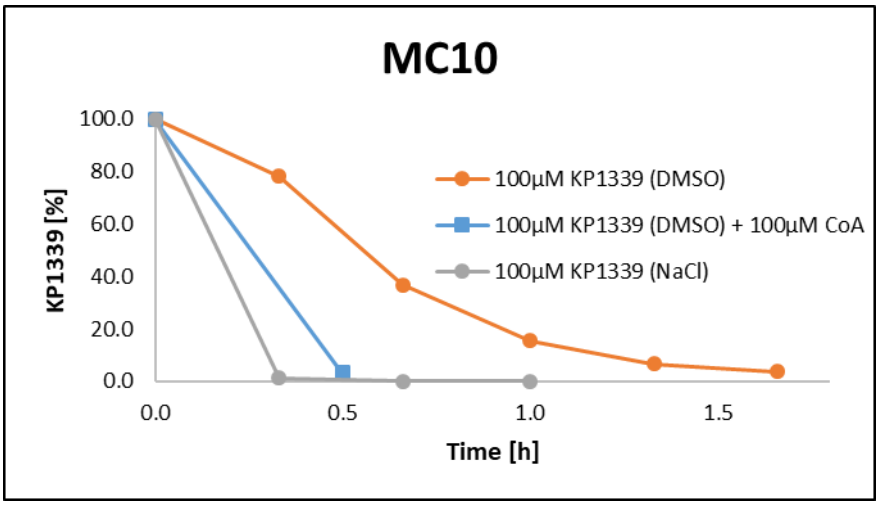

Figure 20: Comparison of protein binding kinetics of KP1339 in MC10 (+CoA)

By adding CoA to MC0 and PBS low-molecular substances containing ruthenium were formed over time. Figure 21 and Figure 22 show these substances at different injection times.

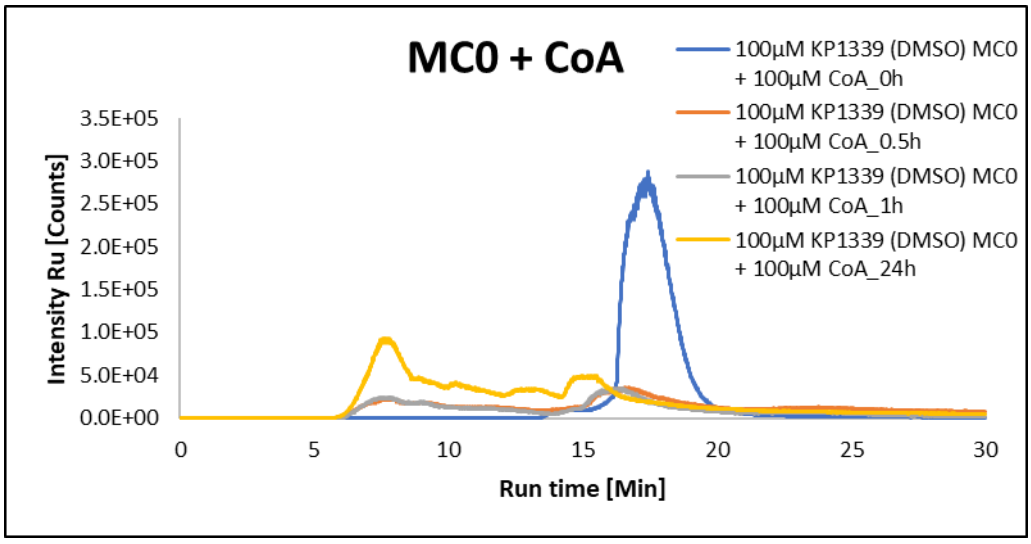

Figure 21: Chromatogram KP1339 DMSO stock solution in MC0 + CoA

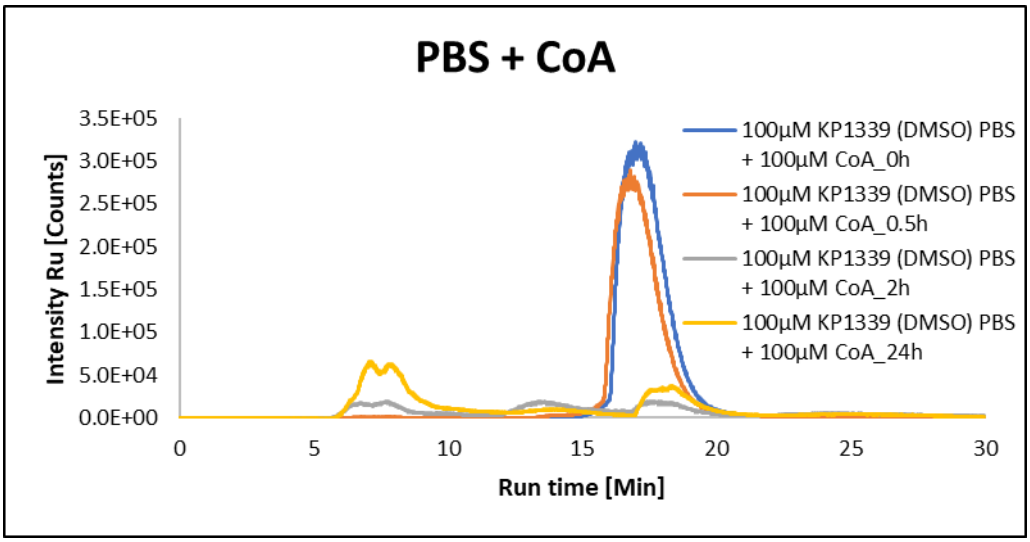

Figure 22: Chromatogram KP1339 DMSO stock solution in PBS + CoA

3.1.2.5 Kinetics measurements with spiked matrices

In MC0 different Ru peaks compared to serum containing cell culture medium were observed due to the absence of albumin. Therefore, in a further approach MC0 was spiked with BSA or FFBSA. The influence of the addition of oleic acid bovine serum albumin (OA BSA) to MC0 or PBS was also investigated.

Figure 23 and Figure 24 show chromatograms of the KP1339 DMSO and NaCl stock solution in MC0 spiked with FFBSA or BSA at different injection times. It becomes apparent that also in albumin spiked MC0 some low-molecular substances containing Ru were developed.

In Figure 23, chromatograms of the two stock solutions in MC0 + FFBSA at different injection times are compared. It seems that fewer of these low-molecular substances are present in the NaCl stock solution than in the DMSO stock solution.

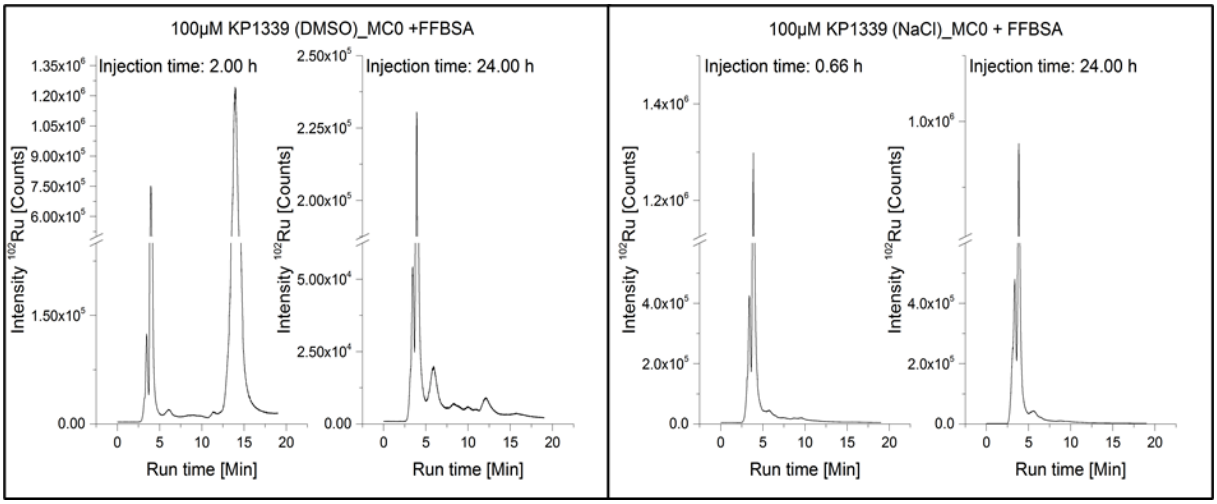

Figure 23: Chromatogram KP1339 DMSO and NaCl stock solution in MC0 + FFBSA, comparison of different injection times

Figure 24 shows chromatograms for both stock solutions in MC0 + BSA. Again, there are fewer of these compounds in the KP1339 NaCl stock solution.

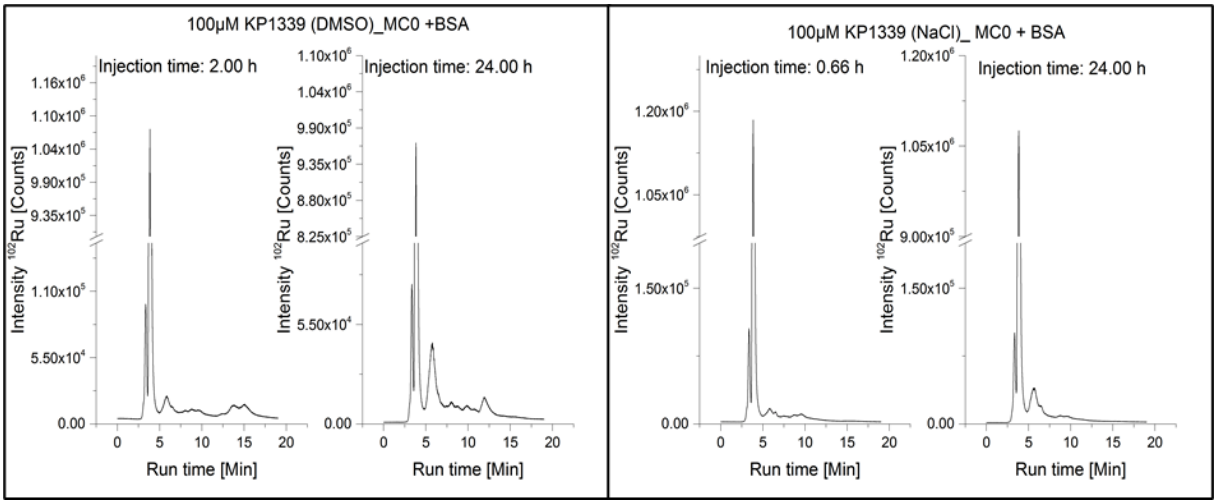

Figure 24: Chromatogram KP1339 DMSO and NaCl stock solution in MC0 + BSA, comparison different injection times

The comparison of the KP1339 DMSO and the 0.9 % NaCl stock solution in MC0/PBS + OA BSA is shown in the following Figure. The decrease of KP1339 is plotted against time. The protein binding kinetics is much faster in MC0 + OA BSA than in PBS + OA BSA.

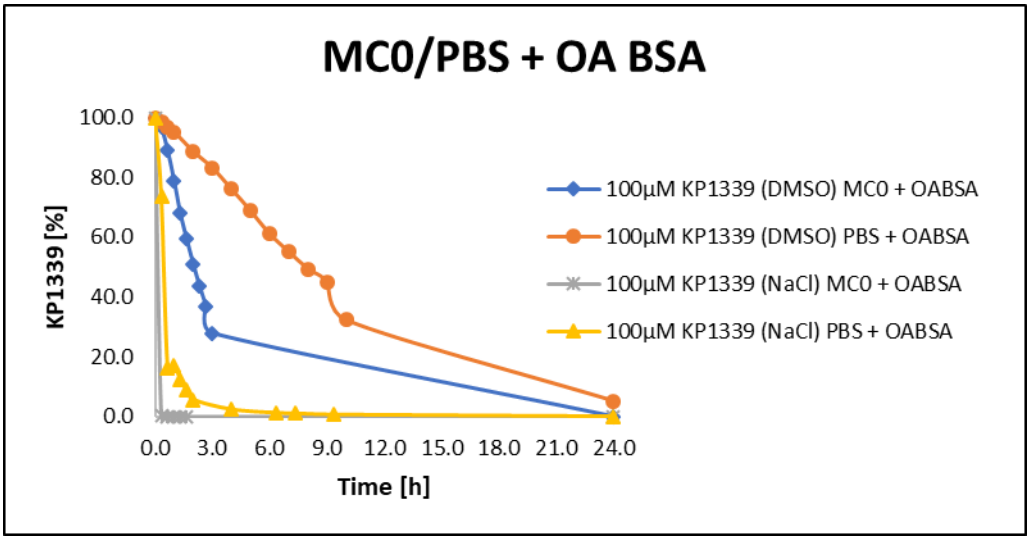

Figure 25: Kinetics measurements KP1339 DMSO and NaCl stock solution in MC0/PBS + OA BSA

In Figure 26, chromatograms of the KP1339 DMSO and NaCl stock solution in PBS + OA BSA are shown. In the DMSO stock solution, there is still some free KP1339 left after 24 hours and in the NaCl stock solution, there is no free KP1339 left.

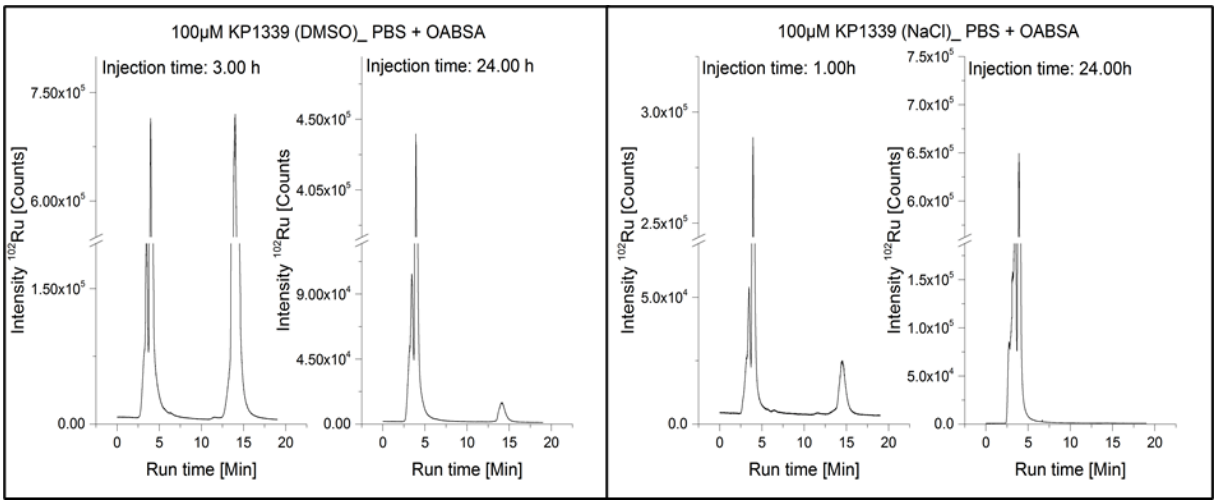

Figure 26: Chromatogram KP1339 DMSO and NaCl stock solution in PBS + OA BSA, comparison different injection times

In MC0 + OA BSA were some low-molecular substances formed (Figure 27).

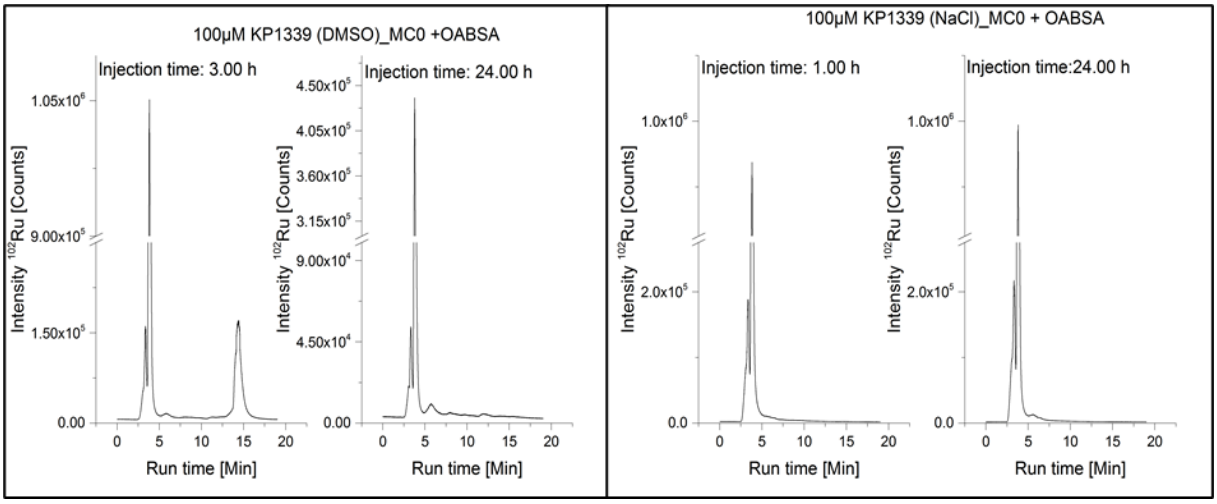

Figure 27: Chromatogram KP1339 DMSO and NaCl stock solution in MC0 + OA BSA, comparison different injection times

Figure 25 showed that the kinetics in MC0 + OA BSA were faster than in PBS + OA BSA. The representation refers to the decrease of KP1339 over time. However, different Ru compounds are formed in various media (e.g. MC0) as shown in Figure 27. Due to the formation

of additional compounds, the amount of KP1339 decreases faster and thus it seems that the protein binding kinetics is accelerated. Especially in complex media, it is advisable to present the results in different ways.

In Figure 28, the protein binding kinetics of the KP1339 DMSO and NaCl stock solution in MC0 spiked with FFBSA, BSA, and OA BSA are shown. KP1339 dissolved in 0.9 % NaCl binds so fast that no difference between MC0 + FFBSA/BSA/OA BSA can be observed. Thus, no conclusion can be drawn in the KP1339 NaCl stock solution about a possible influence of the fat content on the binding. In the KP1339 DMSO stock solution, no trend regarding the fat content can be detected either.

In cell culture, an influence of the fat content was observed. Nevertheless, no general influence of the fat content on the kinetics can be drawn. This would require further experiments, which would also include different fatty acids. To investigate whether certain fatty acids have an influence.

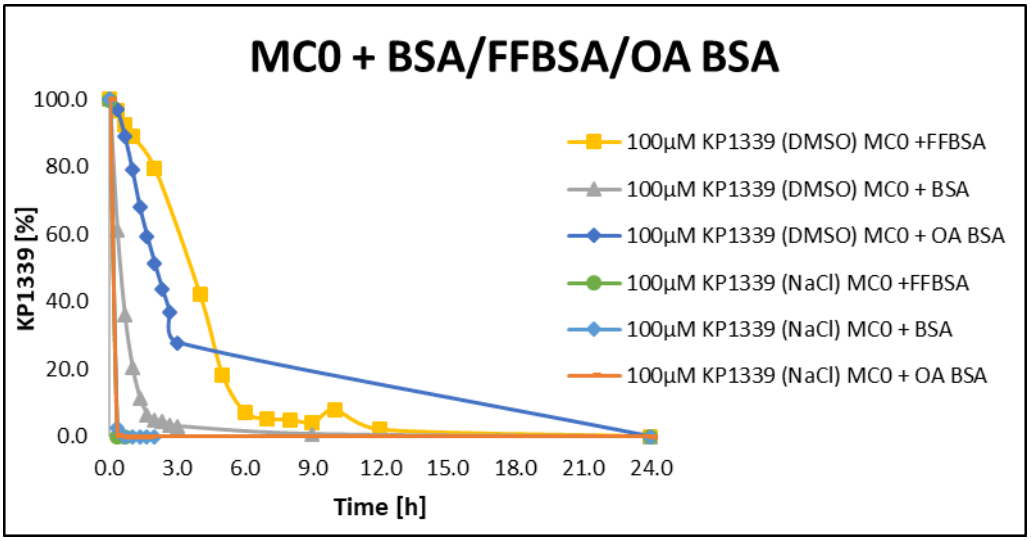

Figure 28: Kinetics measurements KP1339 DMSO and NaCl stock in MC0 spiked

3.1.3 Mice serum samples and blood pellets

The *in vivo* behavior of KP1339 was investigated in blood pellets and serum samples from mice treated with KP1339. In Table 20, the details for the therapy of the mice are listed. The given dose was for all mice the same, 30 mg/kg twice a week with an interval of three days. The treatment was carried out for two weeks and the samples were taken 24 hours after the last treatment. For the injection, the serum was first incubated 1:1 with KP1339 or 0.9 % NaCl and only then the administration was carried out. The HCT116res colon cancer cell line was used, which was bred to be resistant to KP1339. Four mice were treated with KP1339 and the same number was treated with KP1339/etomoxir. Two mice were used as control mice (mouse 7 and 8), which did not receive KP1339.

Table 20: *In vivo* samples of the treated mice

Mouse	Theraphy i.v./i.p.
mouse 3_KP1339	4x i.v. 1:1 serum:KP1339 daily i.p. NaCl
mouse 4_KP1339	4x i.v. 1:1 serum:KP1339 daily i.p. NaCl
mouse 5_KP1339	4x i.v. 1:1 serum:KP1339 daily i.p. NaCl
mouse 6_KP1339	4x i.v. 1:1 serum:KP1339 daily i.p. NaCl
mouse 7_control	4x i.v. 1:1 serum:NaCl daily i.p. NaCl
mouse 8_control	4x i.v. 1:1 serum:NaCl daily i.p. etomoxir
mouse 13_ KP1339/etomoxir	4x i.v. 1:1 serum:KP1339 daily i.p. etomoxir
mouse 14_ KP1339/etomoxir	4x i.v. 1:1 serum:KP1339 daily i.p. etomoxir
mouse 15_ KP1339/etomoxir	4x i.v. 1:1 serum:KP1339 daily i.p. etomoxir
mouse 16_ KP1339/etomoxir	4x i.v. 1:1 serum:KP1339 daily i.p. etomoxir

3.1.3.1 Ruthenium content in mice blood pellets and serum samples

In Table 21 the ruthenium concentrations, which were determined in the blood pellets and serum samples of mice treated with KP1339 and KP1339/etomoxir, are listed. All values are blank corrected, and the dilution factor was included in the calculation. As expected, no ruthenium was detected in the two control mice

Table 21: Ruthenium concentrations in mice blood pellets and serum samples

	Blood pellet	Serum
Sample	**Ru conc. [mg/kg]**	**Ru conc. [mg/kg]**
mouse 3_KP1339	20.59	22.28
mouse 4_KP1339	10.59	15.66
mouse 5_KP1339	2.70	4.35
mouse 6_KP1339	28.87	15.38
mouse 7_control	<LOQ	<LOQ
mouse 8_control	<LOQ	<LOQ
mouse 13_KP1339/etomoxir	20.72	26.35
mouse 14_ KP1339/etomoxir	10.04	7.83
mouse 15_ KP1339/etomoxir	10.46	21.77
mouse 16_ KP1339/etomoxir	22.60	27.34

Due to the large variation of the Ru content in the blood pellet and serum from the same treatment group, it is difficult to draw conclusions. Possible fluctuations in the ruthenium content could be due to a less than optimal therapy or that the dose was not injected well. This can be seen in the samples of mouse 5, which showed significantly lower Ru levels compared to the other samples. Blood pellet and serum of mice treated with KP1339 showed Ru concentrations between 10-30 mg/kg and 15-22 mg/kg, respectively. For mice samples treated with a combination of KP1339/Etomoxir, similar Ru levels could be observed. Blood pellets showed a Ru concentration between 10-20 mg/kg and serum a Ru concentration between 20-27 mg/kg. In general, high Ru levels were found in serum indicating that KP1339 is bound to albumin and circulating in the bloodstream, which is favourable for the compound delivery to the tumour site.

3.1.3.2 Investigation of the protein binding of KP1339 in serum samples of mice

In order to investigate, whether the high Ru levels in serum correspond to free KP1339 or KP1339 bound to serum albumin and/or other serum proteins, SEC-ICP-MS measurements were carried out in serum samples of mice treated with KP1339 and with KP1339/etomoxir. Control mice were included as comparison, but no ruthenium was detectable in their serum

samples (data not shown). The investigation of the protein binding via SEC-ICP-MS in treated samples showed that no free KP1339 was present. In Figure 29 and Figure 30 chromatograms from KP1339 treated mice, and the KP1339 + etomoxir treated mice are shown. Blue is the ruthenium trace and red is the sulphur trace. There is no discernible difference in the binding of KP1339 or KP1339/etomoxir treated mice.

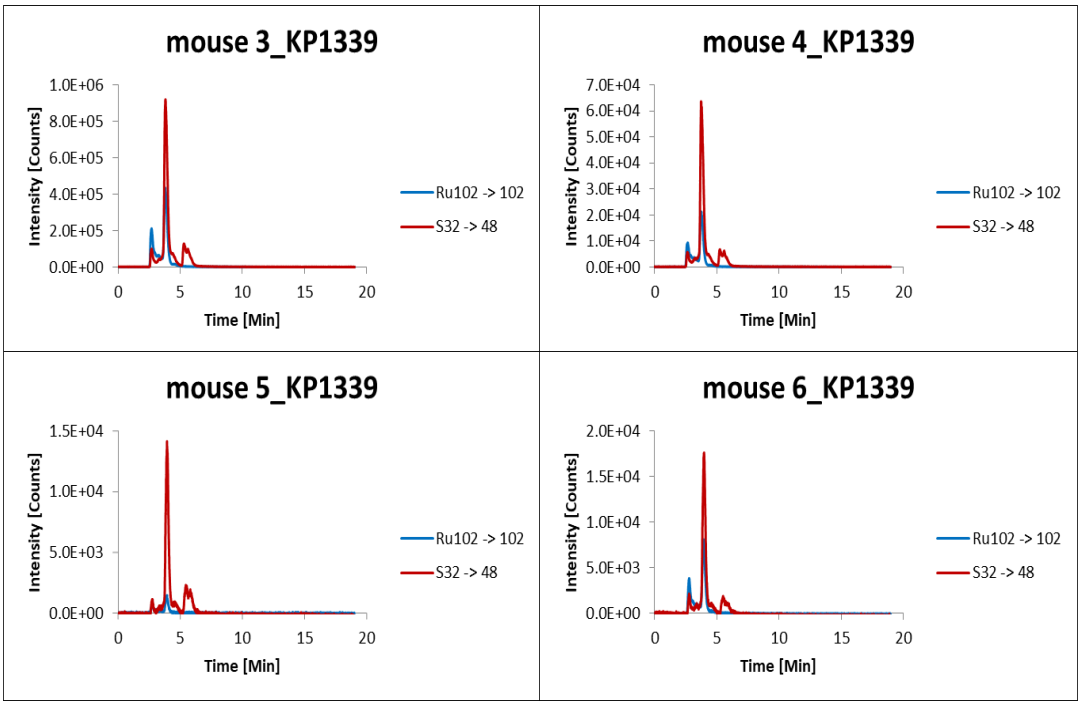

Figure 29: Chromatograms mouse serum samples, mouse 3-6_KP1339

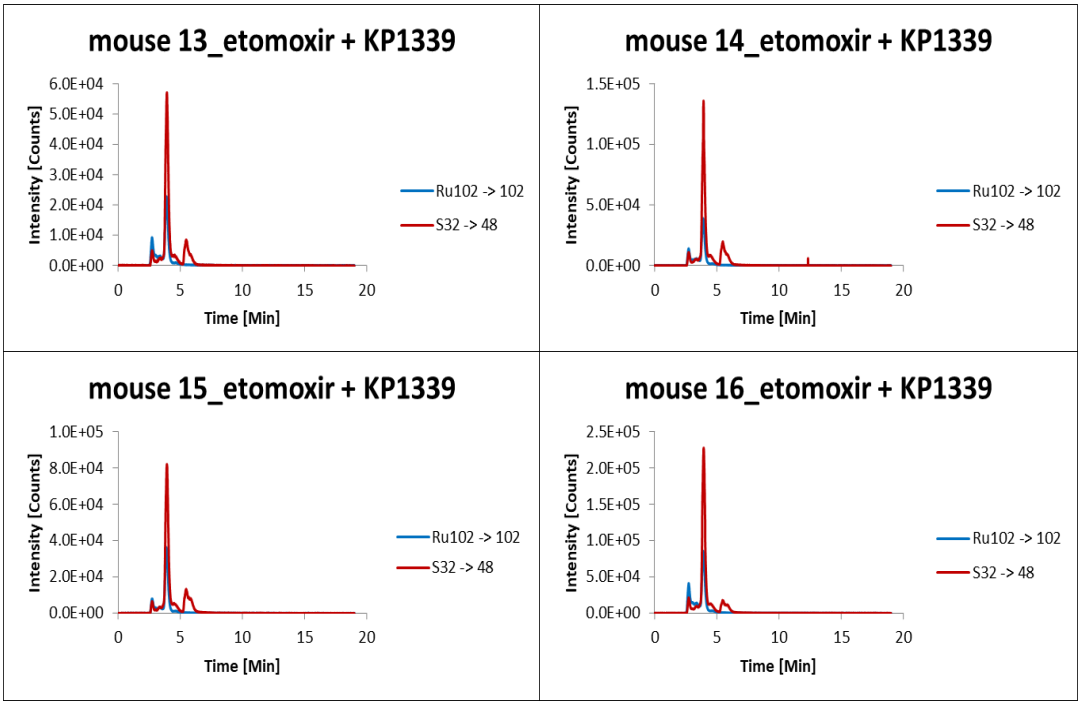

Figure 30: Chromatograms mouse serum samples, mouse 13-16_etomoxir + KP1339

3.2 ESI-MS

Due to the complete atomisation of the sample in the ICP, no conclusion can be drawn about the composition of a compound. However, it is possible to obtain information about the molecular composition in organic mass spectrometry. Therefore, it was possible to detect some compounds that are formed instead of or in addition to the binding to albumin. However, quantification is not possible with this method due to numerous factors e.g. ion suppression.

3.2.1 Stability measurements

For the stability study, the KP1339 0.9 % NaCl stock solution was diluted with 0.9 % NaCl to an end concentration of 400 µM. In the process, KP1339 was dissolved either by vortexing or by the ultrasonic bath. A pH value of seven was determined for the sample that was dissolved by vortexing. Since it was shown in other test series that the stability of KP1339 is significantly better in an acidic medium, the pH value was adjusted to three for a dilution.

Besides KP1339, other compounds with ruthenium have been traced in all three stability approaches. These compounds do not necessarily have to come from the dissolution process because the can be a result of the ion source.

No quantification is possible by ESI-MS, but a trend can still be identified. By comparing the peak area of KP1339 the stability depends on the temperature. The area of the sample that was stored at 37 degrees Celsius decreases significantly over time compared to the sample that was cooled. Nevertheless, it can be said that the stability is significantly better when the sample is refrigerated. This could be observed in all three approaches (ultrasonic bath, vortexing pH ~ 7, vortexing pH ~ 3).

In Figure 31 chromatograms of KP1339 (NaCl stock solution) in 0.9 % NaCl are shown. Which was dissolved by vortexing and the pH was adjusted to three. It is noticeable that the KP1339 peak after 24 hours at 37 degrees Celsius (B) is significantly lower compared to the sample which was stored at 4 degrees Celsius (C).

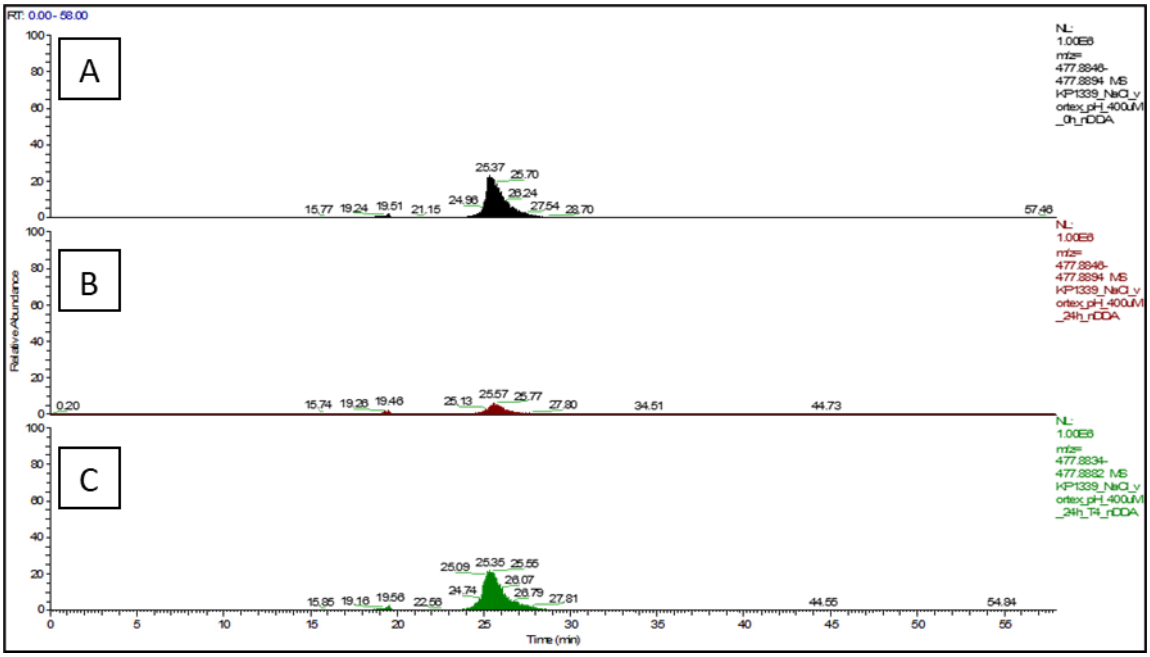

Figure 31: Chromatogram of KP1339 (NaCl) in 0.9% NaCl, vortexing, pH ~3, fixed scale

A: injection time 0h, r.t.; B: injection time 24h, 37°C; C: injection time 24h, 4°C

3.2.2 Kinetics measurements

For the kinetics measurements, KP1339 was dissolved in DMSO and MC0 and afterwards diluted with MC10 and/or MC0.

First test measurements were carried out with a lower initial concentration and injection volume. However, increasing the initial KP1339 concentration and a larger injection volume showed that more ruthenium isotopes could be detected. The first measurement was carried out directly after the sample preparation. This was followed by measurements after one, two, three, four, and 24 hours. Besides, one measurement was taken after five or 25 hours with a wider isolation window to get hold of all ruthenium isotopes. The measurements were carried out in positive and negative mode.

KP1339 was hardly soluble in MC0. Even after vortexing and treatment in an ultrasonic bath, some solid remained. Although the liquid supernatant was further used, the peak of KP1339 was much lower than in the DMSO stock solution. Due to the low intensity and the missing isotopic pattern, the data could not be interpreted further. Therefore, only the results of the KP1339 DMSO stock solution will be discussed in the following.

By measuring the KP1339 stock solution in MC0 and MC10 by organic mass spectrometry, numerous adducts were detected. For the possible candidates, the isotopic pattern was generated and compared with the results of the measurement. Furthermore, the theoretical

sum formula was generated for the respective m/z value. Thus, the adducts were confirmed in two ways.

3.2.2.1 KP1339 in MC0

In MC0, numerous peaks with an isotopic pattern of ruthenium were observed. Especially adducts with DMSO and amino acids could be detected. Such compounds were detected in the measurement in negative and positive mode.

For the formation of adducts of the type $Ru_1L_2Cl_1DMSO_1AA_1$ (Figure 32), three chlorine atoms are split off. For the adduct to be negatively charged and thus measurably in the negative mode, other components must bind to the reduced central atom. In addition to the negative chlorine, a doubly deprotonated amino acid binds, making the entire complex single negatively charged. The neutral DMSO does not contribute any charge.

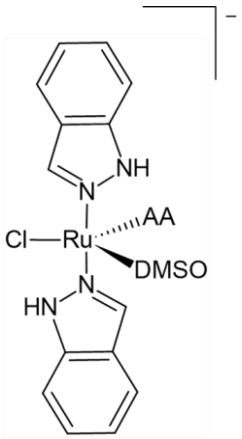

Figure 32: Structure of $Ru_1L_2Cl_1DMSO_1AA_1$

In Figure 33 adducts of this type are shown. The data were normalised and then plotted against the injection time points. The intensity of the respective adduct increases over time.

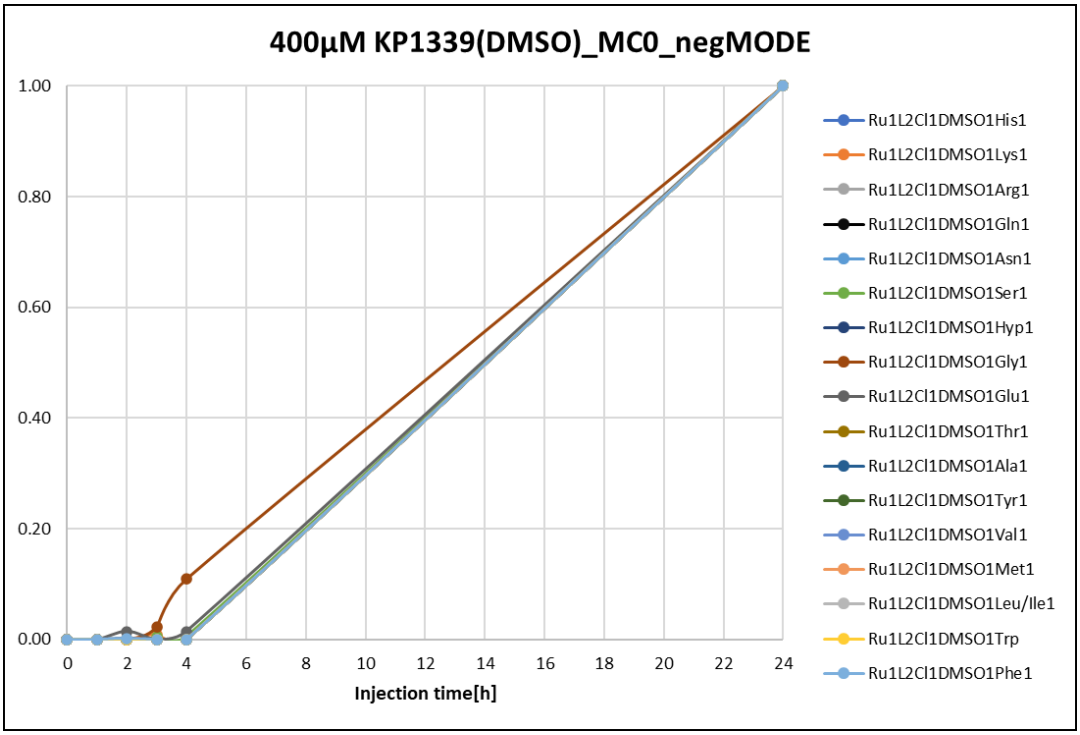

Figure 33: Adduct formation ($Ru_1L_2Cl_1DMSO_1AA_1$) in KP1339 (DMSO) in MC0_neg. Mode

For the $Ru_1L_2DMSO_2AA_1$ adducts, the amino acid is triple deprotonated, thus the complex receives a negative charge. Adducts with two DMSO were detected significantly less. In Figure 34 the normalised data plotted against the various injection times are shown.

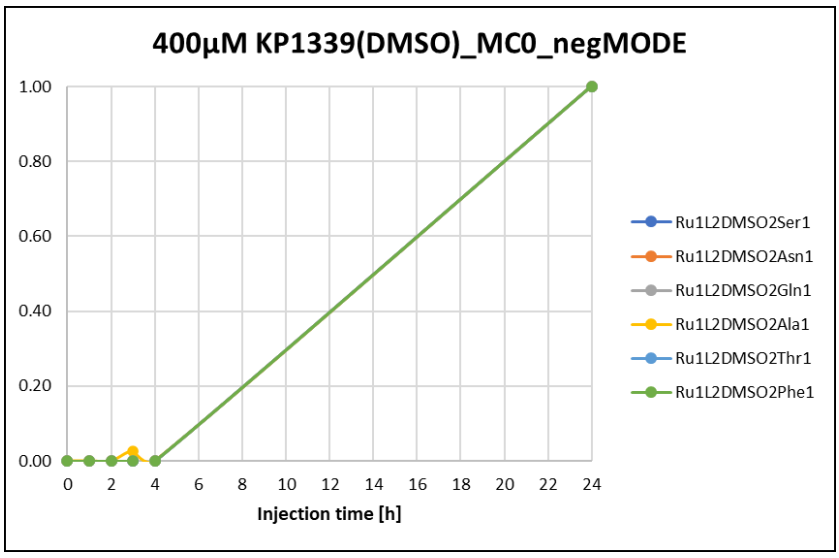

Figure 34: Adduct formation ($Ru_1L_2DMSO_2AA_1$) in KP1339 (DMSO) in MC0_neg. Mode

In the positive mode, most $Ru_1L_2Cl_1DMSO_1AA_1$ adducts that were previously confirmed in the negative mode were also detected. The results for $Ru_1L_2Cl_1DMSO_1AA_1$ adducts are shown in

Figure 35. In the positive mode, the amino acid hydroxyproline could not be detected. For it, an adduct with aspartic acid could be verified.

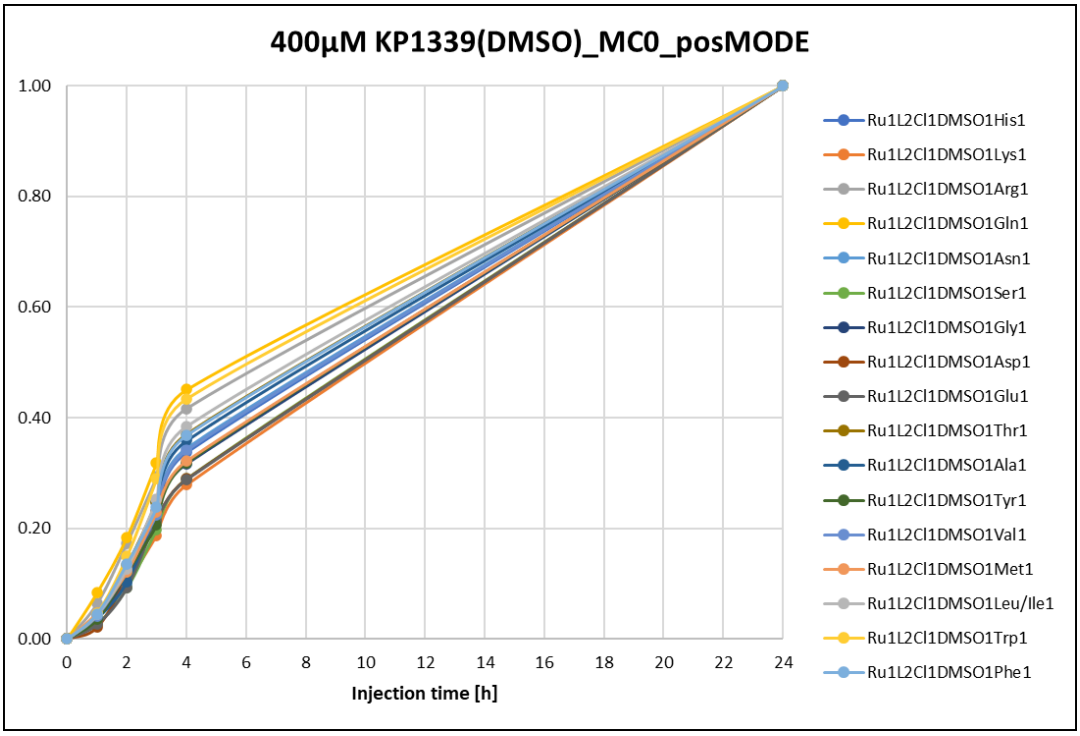

Figure 35: Adduct formation ($Ru_1L_2Cl_1DMSO_1AA_1$) in KP1339 (DMSO) in MC0_pos. Mode

The normalised data for the $Ru_1L_2DMSO_2AA_1$ adducts in the positive mode are given in Figure 36. Ten more adducts were detected in the positive mode than in the negative mode. The adduct with the amino acid asparagine could not be detected in the positive mode.

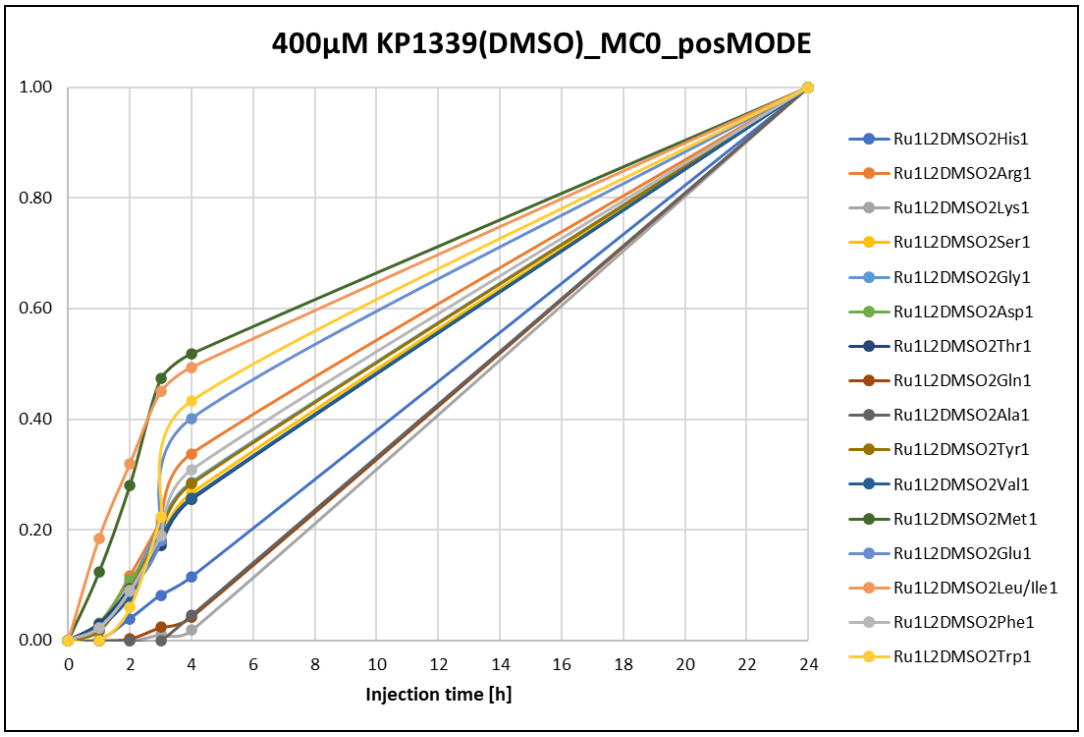

Figure 36: Adduct formation ($Ru_1L_2DMSO_2AA_1$) in KP1339 (DMSO) in MC0_pos. Mode

In the following table (Table22), all adducts are listed, which were confirmed in MC0. The adducts are ordered according to their retention time.

Table 22: List of formed adducts in KP1339 (DMSO) in MC0

No	$Ru_1L_2Cl_1DMSO_1AA_1$ adducts		$Ru_1L_2DMSO_2AA_1$ adducts	
	MC0		MC0	
	negative Mode	positive Mode	negative Mode	positive Mode
1	$Ru_1L_2Cl_1DMSO_1His_1$	$Ru_1L_2Cl_1DMSO_1His_1$	$Ru_1L_2DMSO_2Ser_1$	$Ru_1L_2DMSO_2His_1$
2	$Ru_1L_2Cl_1DMSO_1Lys_1$	$Ru_1L_2Cl_1DMSO_1Lys_1$	$Ru_1L_2DMSO_2Asn_1$	$Ru_1L_2DMSO_2Arg_1$
3	$Ru_1L_2Cl_1DMSO_1Arg_1$	$Ru_1L_2Cl_1DMSO_1Arg_1$	$Ru_1L_2DMSO_2Gln_1$	$Ru_1L_2DMSO_2Lys_1$
4	$Ru_1L_2Cl_1DMSO_1Gln_1$	$Ru_1L_2Cl_1DMSO_1Gln_1$	$Ru_1L_2DMSO_2Ala_1$	$Ru_1L_2DMSO_2Ser_1$
5	$Ru_1L_2Cl_1DMSO_1Asn_1$	$Ru_1L_2Cl_1DMSO_1Asn_1$	$Ru_1L_2DMSO_2Thr_1$	$Ru_1L_2DMSO_2Gly_1$
6	$Ru_1L_2Cl_1DMSO_1Ser_1$	$Ru_1L_2Cl_1DMSO_1Ser_1$	$Ru_1L_2DMSO_2Phe_1$	$Ru_1L_2DMSO_2Asp_1$
7	$Ru_1L_2Cl_1DMSO_1Hyp_1$	$Ru_1L_2Cl_1DMSO_1Gly_1$		$Ru_1L_2DMSO_2Thr_1$
8	$Ru_1L_2Cl_1DMSO_1Gly_1$	$Ru_1L_2Cl_1DMSO_1Asp_1$		$Ru_1L_2DMSO_2Gln_1$
9	$Ru_1L_2Cl_1DMSO_1Glu_1$	$Ru_1L_2Cl_1DMSO_1Glu_1$		$Ru_1L_2DMSO_2Ala_1$
10	$Ru_1L_2Cl_1DMSO_1Thr_1$	$Ru_1L_2Cl_1DMSO_1Thr_1$		$Ru_1L_2DMSO_2Tyr_1$
11	$Ru_1L_2Cl_1DMSO_1Ala_1$	$Ru_1L_2Cl_1DMSO_1Ala_1$		$Ru_1L_2DMSO_2Val_1$
12	$Ru_1L_2Cl_1DMSO_1Tyr_1$	$Ru_1L_2Cl_1DMSO_1Tyr_1$		$Ru_1L_2DMSO_2Met_1$
13	$Ru_1L_2Cl_1DMSO_1Val_1$	$Ru_1L_2Cl_1DMSO_1Val_1$		$Ru_1L_2DMSO_2Glu_1$
14	$Ru_1L_2Cl_1DMSO_1Met_1$	$Ru_1L_2Cl_1DMSO_1Met_1$		$Ru_1L_2DMSO_2Leu/Ile_1$
15	$Ru_1L2Cl_1DMSO_1Leu/Ile_1$	$Ru_1L_2Cl_1DMSO_1Leu/Ile_1$		$Ru_1L_2DMSO_2Phe_1$
16	$Ru_1L_2Cl_1DMSO_1Trp_1$	$Ru_1L_2Cl_1DMSO_1Trp_1$		$Ru_1L_2DMSO_2Trp_1$
17	$Ru_1L_2Cl_1DMSO_1Phe_1$	$Ru_1L_2Cl_1DMSO_1Phe_1$		

When comparing Figure 33, Figure 34, Figure 35, and Figure 36, it can be seen that the intensity of the adducts is highest after 24 hours in both the negative and the positive mode.

3.2.2.2 KP1339 in MC10

Just as in MC0, various adducts with amino acids and DMSO were formed in MC10 in combination with KP1339.

In Figure 37 the adducts which in addition to the ruthenium and two indazoles, contain one chlorine, one DMSO, and one amino acid are shown. The data were normalised and then plotted against the injection time points. These are the data obtained in the negative mode. In the process, the intensity of the adducts increases over time.

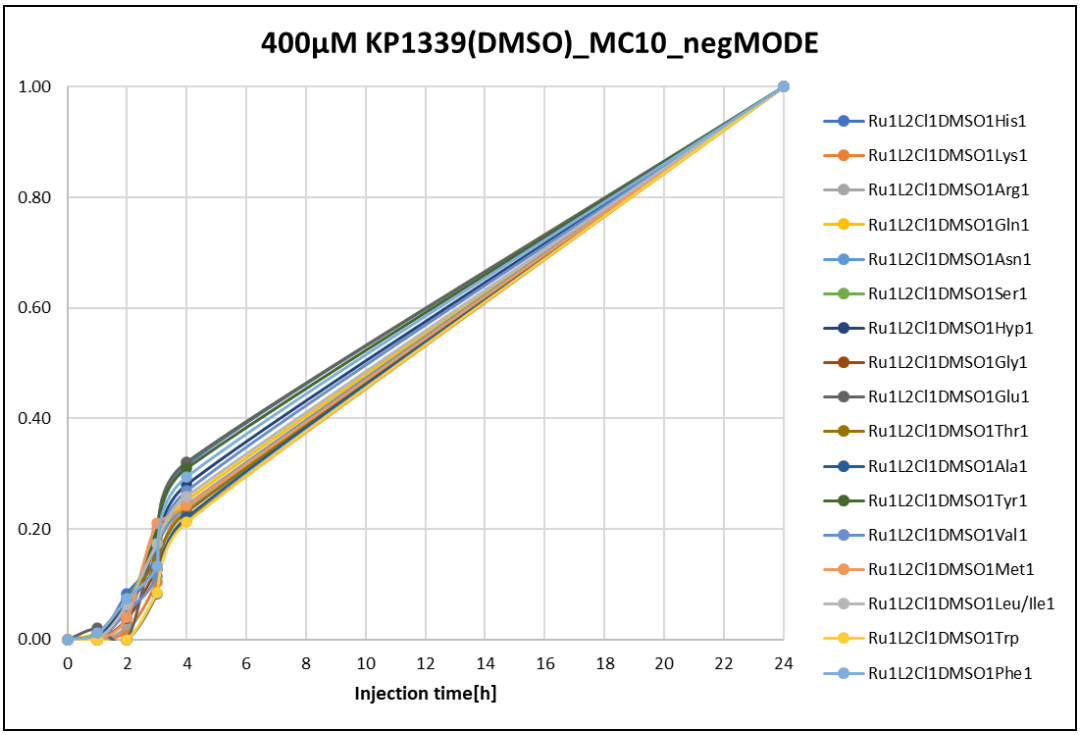

Figure 37: Adduct formation ($Ru_1L_2Cl_1DMSO_1AA_1$) in KP1339 (DMSO) in MC10_neg. Mode

The number of adducts of type $Ru_1L_2DMSO_2AA_1$ are significantly lower compared to $Ru_1L_2Cl_1DMSO_1AA_1$. In Figure 38 the adducts with two DMSO, which were detected in the negative mode, are shown.

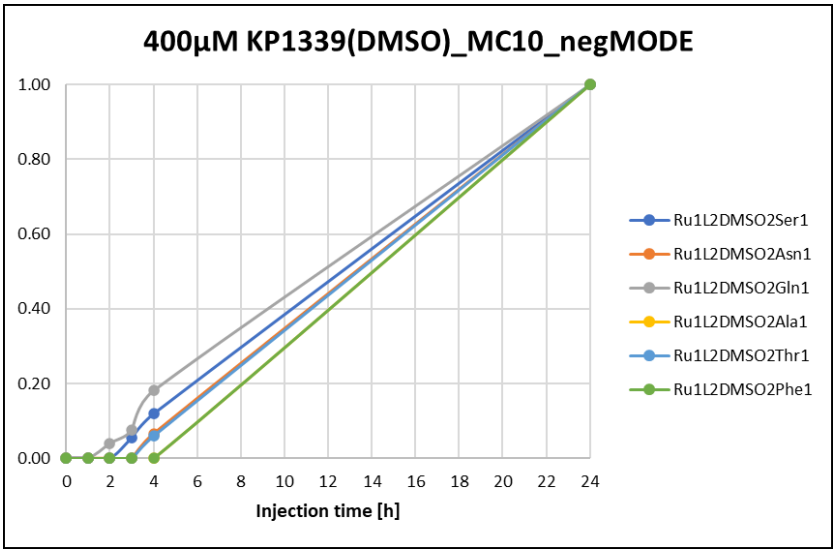

Figure 38: Adduct formation ($Ru_1L_2DMSO_2AA_1$) in KP1339 (DMSO) in MC10_neg. Mode

In the positive mode, almost all $Ru_1L_2Cl_1DMSO_1AA_1$ adducts could be detected that were also identified in the negative mode. However, the adduct with hydroxyproline could not be detected, but an adduct with aspartic acid was identified.

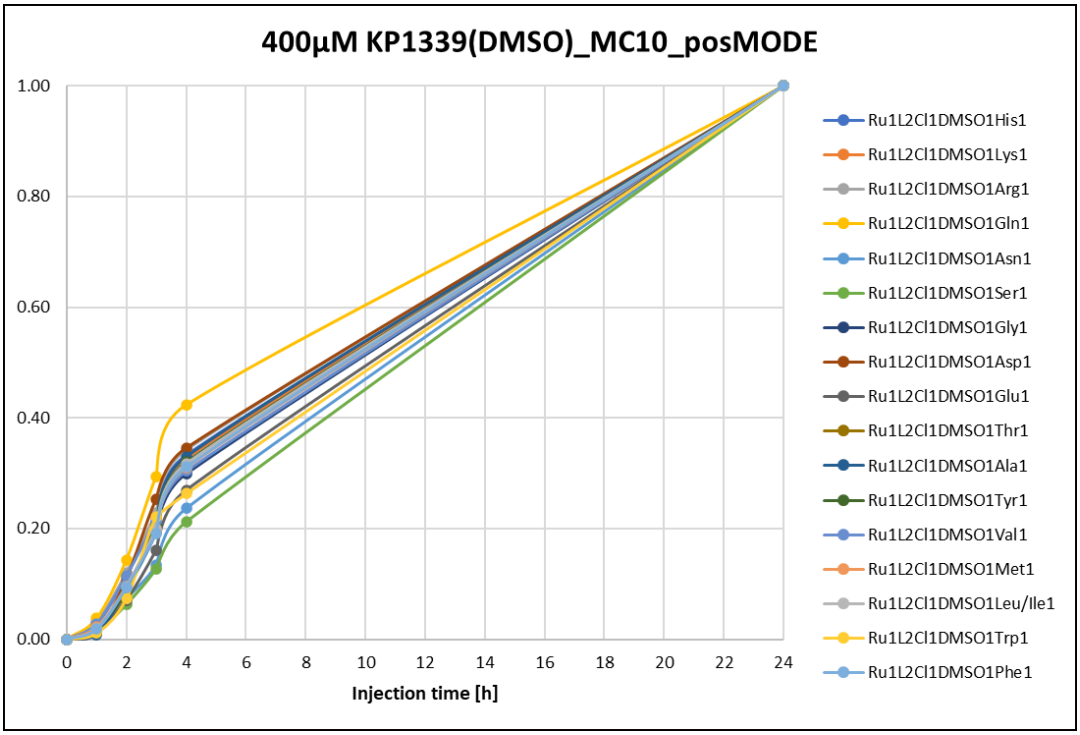

Figure 39: Adduct formation ($Ru_1L_2Cl_1DMSO_1AA_1$) in KP1339 (DMSO) in MC10_pos. Mode

The normalised data for the $Ru_1L_2DMSO_2AA_1$ adducts in the positive mode are given in Figure 40. By comparison with the results of the measurements in the negative mode, more ad-

ducts with two DMSO were detected in the positive mode. The adduct with the amino acid asparagine could not be detected in the positive mode.

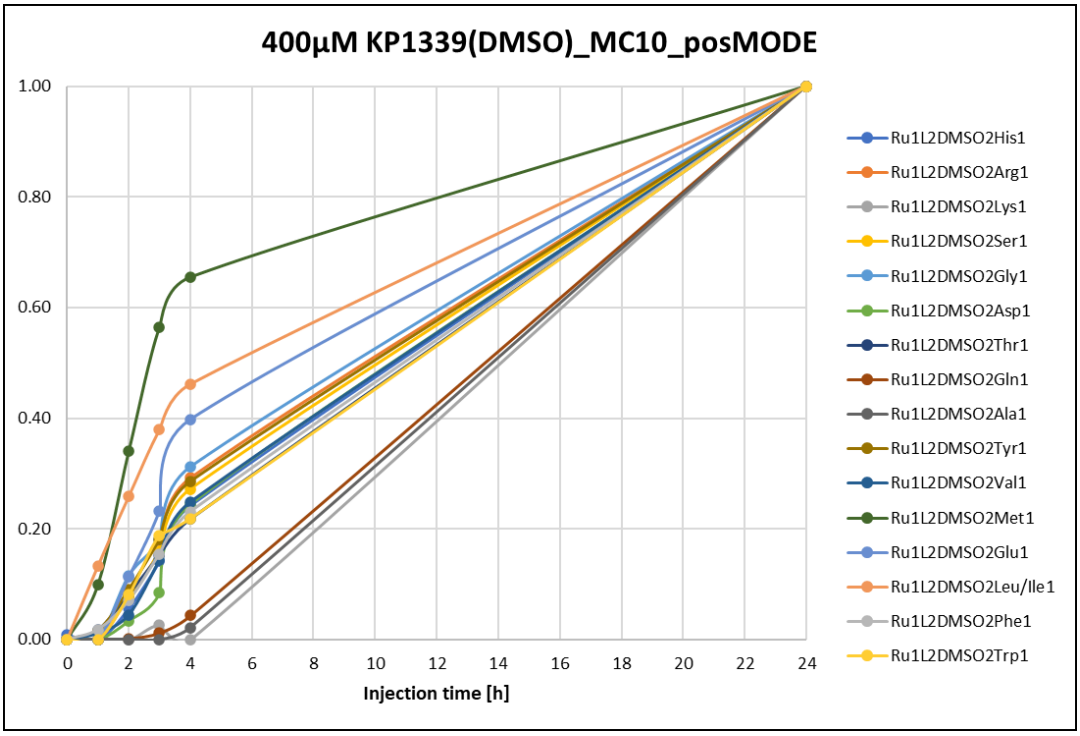

Figure 40: Adduct formation ($Ru_1L_2DMSO_2AA_1$) in KP1339 (DMSO) in MC10_pos. Mode

In the following table (Table 23), all adducts detected in MC10 are listed according to their retention time. The same compounds were detected in MC0 (Table 22).

Table 23: List of formed adducts in KP1339 (DMSO) in MC10

No	$Ru_1L_2Cl_1DMSO_1AA_1$ adducts		$Ru_1L_2DMSO_2AA_1$ adducts	
	MC10		MC10	
	negative Mode	positive Mode	negative Mode	positive Mode
1	$Ru_1L_2Cl_1DMSO_1His_1$	$Ru_1L_2Cl_1DMSO_1His_1$	$Ru_1L_2DMSO_2Ser_1$	$Ru_1L_2DMSO_2His_1$
2	$Ru_1L_2Cl_1DMSO_1Lys_1$	$Ru_1L_2Cl_1DMSO_1Lys_1$	$Ru_1L_2DMSO_2Asn_1$	$Ru_1L_2DMSO_2Arg_1$
3	$Ru_1L_2Cl_1DMSO_1Arg_1$	$Ru_1L_2Cl_1DMSO_1Arg_1$	$Ru_1L_2DMSO_2Gln_1$	$Ru_1L_2DMSO_2Lys_1$
4	$Ru_1L_2Cl_1DMSO_1Gln_1$	$Ru_1L_2Cl_1DMSO_1Gln_1$	$Ru_1L_2DMSO_2Ala_1$	$Ru_1L_2DMSO_2Ser_1$
5	$Ru_1L_2Cl_1DMSO_1Asn_1$	$Ru_1L_2Cl_1DMSO_1Asn_1$	$Ru_1L_2DMSO_2Thr_1$	$Ru_1L_2DMSO_2Gly_1$
6	$Ru_1L_2Cl_1DMSO_1Ser_1$	$Ru_1L_2Cl_1DMSO_1Ser_1$	$Ru_1L_2DMSO_2Phe_1$	$Ru_1L_2DMSO_2Asp_1$
7	$Ru_1L_2Cl_1DMSO_1Hyp_1$	$Ru_1L_2Cl_1DMSO_1Gly_1$		$Ru_1L_2DMSO_2Thr_1$
8	$Ru_1L_2Cl_1DMSO_1Gly_1$	$Ru_1L_2Cl_1DMSO_1Asp_1$		$Ru_1L_2DMSO_2Gln_1$
9	$Ru_1L_2Cl_1DMSO_1Glu_1$	$Ru_1L_2Cl_1DMSO_1Glu_1$		$Ru_1L_2DMSO_2Ala_1$
10	$Ru_1L_2Cl_1DMSO_1Thr_1$	$Ru_1L_2Cl_1DMSO_1Thr_1$		$Ru_1L_2DMSO_2Tyr_1$
11	$Ru_1L_2Cl_1DMSO_1Ala_1$	$Ru_1L_2Cl_1DMSO_1Ala_1$		$Ru_1L_2DMSO_2Val_1$
12	$Ru_1L_2Cl_1DMSO_1Tyr_1$	$Ru_1L_2Cl_1DMSO_1Tyr_1$		$Ru_1L_2DMSO_2Met_1$
13	$Ru_1L_2Cl_1DMSO_1Val_1$	$Ru_1L_2Cl_1DMSO_1Val_1$		$Ru_1L_2DMSO_2Glu_1$
14	$Ru_1L_2Cl_1DMSO_1Met_1$	$Ru_1L_2Cl_1DMSO_1Met_1$		$Ru_1L_2DMSO_2Leu/Ile_1$
15	$Ru_1L_2Cl_1DMSO_1Leu/Ile_1$	$Ru_1L_2Cl_1DMSO_1Leu/Ile_1$		$Ru_1L_2DMSO_2Phe_1$
16	$Ru_1L_2Cl_1DMSO_1Trp_1$	$Ru_1L_2Cl_1DMSO_1Trp_1$		$Ru_1L_2DMSO_2Trp_1$
17	$Ru_1L_2Cl_1DMSO_1Phe_1$	$Ru_1L_2Cl_1DMSO_1Phe_1$		

3.2.2.3 Comparison KP1339 in MC0 and MC10

The combination of the KP1339 stock solution and MC0 or MC10 led to the formation of numerous adducts. By comparing the area of KP1339 at time point zero (0 h) and the area of the adducts after 24 hours, it is visible that the adducts occur more intensely in MC0.
In Table 24 the percentages of the formed adducts that have one DMSO are listed. These values can only be used as a guide, as quantification in ESI-MS is not straightforward.

Table 24: Percentage of $Ru_1L_2Cl_1DMSO_1AA_1$ adducts in MC0 and MC10 after 24 hours

	Peak Area				**Percentage adduct [%]**	
	MC0		**MC10**		**MC0**	**MC10**
	0h	**24h**	**0h**	**24h**		
KP1339	164018560	0	50707702	10051		
$Ru_1L_2Cl_1DMSO_1His_1$		1156350		262732	0.71	0.52
$Ru_1L_2Cl_1DMSO_1Lys_1$		1124460		280071	0.69	0.55
$Ru_1L_2Cl_1DMSO_1Arg_1$		1898566		396560	1.16	0.78
$Ru_1L_2Cl_1DMSO_1Gln_1$		9188689		3449391	5.60	6.80
$Ru_1L_2Cl_1DMSO_1Asn_1$		3706181		701745	2.26	1.38
$Ru_1L_2Cl_1DMSO_1Ser_1$		2197239		534807	1.34	1.05
$Ru_1L_2Cl_1DMSO_1Hyp_1$		2591535		450088	1.58	0.89
$Ru_1L_2Cl_1DMSO_1Gly_1$		282170		446370	0.17	0.88
$Ru_1L_2Cl_1DMSO_1Glu_1$		504190		144563	0.31	0.29
$Ru_1L_2Cl_1DMSO_1Thr_1$		1867325		388204	1.14	0.77
$Ru_1L_2Cl_1DMSO_1Ala_1$		772039		236982	0.47	0.47
$Ru_1L_2Cl_1DMSO_1Tyr_1$		1624788		245147	0.99	0.48
$Ru_1L_2Cl_1DMSO_1Val_1$		1378919		307994	0.84	0.61
$Ru_1L_2Cl_1DMSO_1Met_1$		926190		177779	0.56	0.35
$Ru_1L_2Cl_1DMSO_1Leu/Ile_1$		6511596		1445971	3.97	2.85
$Ru_1L_2Cl_1DMSO_1Trp_1$		301570		57683	0.18	0.11
$Ru_1L_2Cl_1DMSO_1Phe_1$		4216630		767489	2.57	1.51
				Sum	24.54	20.30

The adducts with two DMSO (Table 25) occur in MC0 and MC10 only with a small proportion.

Table 25: Percentage of $Ru_1L_2DMSO_2AA_1$ adducts in MC0 and MC10 after 24 hours

	Peak Area				**Percentage adduct [%]**	
	MC0		**MC10**		**MC0**	**MC10**
	0h	**24h**	**0h**	**24h**		
KP1339	164018560	0	50707702	10051		
$Ru_1L_2DMSO_2Ser_1$		725904		129666	0.44	0.26
$Ru_1L_2DMSO_2Asn_1$		525700		87390	0.32	0.17
$Ru_1L_2DMSO_2Gln_1$		1522526		474931	0.93	0.94
$Ru_1L_2DMSO_2Ala_1$		188592		38545	0.11	0.08
$Ru_1L_2DMSO_2Thr_1$		695415		96549	0.42	0.19
$Ru_1L_2DMSO_2Phe_1$		322861		37519	0.20	0.07
				Sum	2.43	1.71

Due to the formation of various adducts, significantly less KP1339 is available for binding to albumin. The complexity of these cell culture media suggests that even more adducts are produced. This requires further evaluation of the data, as well as additional measurements. Due to these results, the study of the protein binding of KP1339 in *in vitro* experiments should be considered with caution.

4 Conclusion

This work successfully demonstrated the possibilities and limitations of size-exclusion chromatography in combination with ICP-MS for the investigation of the stability and protein binding kinetics of the ruthenium-based anticancer compound KP1339. Through the separation, other ruthenium peaks besides the KP1339 albumin adduct could be detected in some settings. Due to the complete atomisation of the compounds in the plasma it was not possible to conclude a sum formula. Through additional measurements with organic MS, unknown compounds could be detected.

Stability measurements were carried out with both, SEC-ICP-MS and RP-ESI-MS. The choice of the temperature plays a significant role in the stability of KP1339. Various end concentrations were tested for the KP1339 DMSO stock solution in 0.9 % NaCl by ICP-MS. At all of them the ruthenium counts decreased over time and at higher concentrations (200 µM & 400 µM) precipitation could be observed. Further stability measurements showed that the ruthenium content in the KP1339 DMSO stock solution remains stable for at least 24 hours when diluted with MC0.
The measurements with organic and inorganic MS showed that the measurement and storage at 37 degrees Celsius leads to a significant decrease of the ruthenium/KP1339 content.

When studying the kinetics of binding to albumin, the initial concentration of KP1339 plays an essential role. For this, KP1339 was dissolved in DMSO and diluted with various media (BSA, FFBSA, MC10, MC10 delipidated) to obtain different concentrations. It was shown that the binding of KP1339 to albumin is faster when a lower KP1339 concentration is present.
The solvent is also a decisive factor. All measurements showed that the kinetics was faster when KP1339 was dissolved in 0.9% NaCl and not in DMSO. Based on these results, the assumption can be made that the protein binding kinetics is significantly faster if no DMSO is present.
The addition of CoA accelerated the binding of KP1339 to albumin. The addition of CoA was only done for the DMSO dissolved KP1339. But this resulted in an almost similarly fast protein binding as in the KP1339 0.9 % NaCl stock solution.
Not only the solvent is important, but also the medium used for the dilution. In both stock solutions (KP1339 (DMSO), KP1339 (0.9% NaCl)), binding to albumin is significantly faster in

MC10 and MC10delip. than in BSA and FFBSA. A higher proportion of FCS also has an accelerating effect on the binding in the KP1339 DMSO stock solution. No influence could be detected with the 0.9 % NaCl stock solution. In MC0, which does not contain albumin, various low-molecular weight substances are formed over time. Even in the spiked MC0 low-molecular weight substances were developed. There is no difference in the protein binding kinetics of the 0.9 % NaCl stock solution in MC0 spiked with FFBSA, BSA, or OA BSA. In contrast differences in the kinetics in the KP1339 DMSO stock could be observed. However, it is not clear whether the fat content influences the kinetics.

The protein binding in the mouse serum was investigated, no free KP1339 was observed. There was no difference in the protein binding between a KP1339 and an etomoxir + KP1339 treated mouse observed.

The organic mass spectrometry in combination with reversed-phase chromatography made it possible to separate numerous ruthenium compounds besides KP1339. In both MC0 and MC10, adducts of the type $Ru_1L_2Cl_1DMSO_1AA_1$ and $Ru_1L_2DMSO_2AA_1$ were detected. Only these measurements revealed that the adducts were also formed in MC10 and not only in MC0. Nevertheless, the amino acid adducts are formed to a greater extent in MC0.

As a general conclusion, it can be said that organic and inorganic mass spectrometry complement each other very well.
Based on these results, one should keep in mind when experimenting with KP1339 in a cell culture medium that not only a binding to albumin occurs but also to a small extent other adducts with the solvent or the medium can be formed.

5 Appendix

Table 26: Composition McCoy`s 5A Medium **[41]**

Components	Molecular Weight	Concentration [mg/L]	mM
Amino Acids			
Glycine	75.0	7.5	0.1
L-Alanine	89.0	13.9	0.15617977
L-Arginine hydrochloride	211.0	42.1	0.19952606
L-Asparagine	132.0	45.0	0.3409091
L-Aspartic acid	133.0	19.97	0.15015037
L-Cysteine	121.0	31.5	0.2603306
L-Glutamic Acid	147.0	22.1	0.15034014
L-Glutamine	146.0	219.2	1.5013698
L-Histidine hydrochloride-H2O	210.0	20.96	0.09980952
L-Hydroxyproline	131.0	19.7	0.15038168
L-Isoleucine	131.0	39.36	0.300458
L-Leucine	131.0	39.36	0.300458
L-Lysine hydrochloride	183.0	36.5	0.19945355
L-Methionine	149.0	14.9	0.099999994
L-Phenylalanine	165.0	16.5	0.1
L-Proline	115.0	17.3	0.15043478
L-Serine	105.0	26.3	0.25047618
L-Threonine	119.0	17.9	0.15042016
L-Tryptophan	204.0	3.1	0.0151960775
L-Tyrosine	181.0	18.1	0.1
L-Valine	117.0	17.6	0.15042736
Vitamins			
Ascorbic Acid	176.0	0.5	0.0028409092
Biotin	244.0	0.2	8.1967213E-4
Choline chloride	140.0	5.0	0.035714287
D-Calcium pantothenate	477.0	0.2	4.1928721E-4
Folic Acid	441.0	10.0	0.022675738
Niacinamide	122.0	0.5	0.0040983604
Nicotinic acid (Niacin)	123.0	0.5	0.0040650405
Para-Aminobenzoic Acid	137.0	1.0	0.00729927
Pyridoxal hydrochloride	204.0	0.5	0.0024509805
Pyridoxine hydrochloride	206.0	0.5	0.0024271845
Riboflavin	376.0	0.2	5.319149E-4
Thiamine hydrochloride	337.0	0.2	5.934718E-4
Vitamin B12	1355.0	2.0	0.0014760147
i-Inositol	180.0	36.0	0.2
Inorganic Salts			
Calcium Chloride (CaCl2) (anhyd.)	111.0	100.0	0.9009009
Magnesium Sulfate (MgSO4-7H2O)	246.0	200.0	0.8130081
Potassium Chloride (KCl)	75.0	400.0	5.3333335
Sodium Bicarbonate (NaHCO3)	84.0	2200.0	26.190475
Sodium Chloride (NaCl)	58.0	6460.0	111.37931
Sodium Phosphate monobasic (NaH2PO4-H2O)	138.0	580.0	4.2028985
Other Components			
Bacto-Peptone		600.0	Infinity
D-Glucose (Dextrose)	180.0	3000.0	16.666666
Glutathione (reduced)	307.0	0.5	0.0016286644
Phenol Red	376.4	10.0	0.026567481

Literature

[1] B. Atil, „Molecular determinants of the Anti-Cancer Activity of Ruthenium Compound KP1339“, dipl, uniwien, wien, 2010.

[2] P. Heffeter *u. a.*, „Intracellular protein binding patterns of the anticancer ruthenium drugs KP1019 and KP1339“, *JBIC J. Biol. Inorg. Chem.*, Bd. 15, Nr. 5, S. 737–748, Juni 2010, doi: 10.1007/s00775-010-0642-1.

[3] A. K. Bytzek *u. a.*, „LC– and CZE–ICP-MS approaches for the in vivo analysis of the anticancer drug candidate sodium trans-[tetrachloridobis(1H-indazole)ruthenate(iii)] (KP1339) in mouse plasma†“, *Metallomics*, Bd. 3, Nr. 10, S. 1049–1055, Okt. 2011, doi: 10.1039/c1mt00055a.

[4] „Serumproteine“. https://www.spektrum.de/lexikon/biologie/serumproteine/61230 (zugegriffen März 04, 2021).

[5] A. K. Bytzek, G. Koellensperger, B. K. Keppler, und C. G. Hartinger, „Biodistribution of the novel anticancer drug sodium trans-[tetrachloridobis(1H-indazole)ruthenate(III)] KP-1339/IT139 in nude BALB/c mice and implications on its mode of action“, *J. Inorg. Biochem.*, Bd. 160, S. 250–255, Juli 2016, doi: 10.1016/j.jinorgbio.2016.02.037.

[6] B. Neuditschko *u. a.*, „Interaction with Ribosomal Proteins Accompanies Stress Induction of the Anticancer Metallodrug BOLD-100/KP1339 in the Endoplasmic Reticulum“, *Angew. Chem. Int. Ed.*, Bd. 60, Nr. 10, S. 5063–5068, 2021, doi: https://doi.org/10.1002/anie.202015962.

[7] R. Trondl, P. Heffeter, C. R. Kowol, M. A. Jakupec, W. Berger, und B. K. Keppler, „NKP-1339, the first ruthenium-based anticancer drug on the edge to clinical application“, *Chem. Sci.*, Bd. 5, Nr. 8, S. 2925–2932, 2014, doi: 10.1039/C3SC53243G.

[8] O. Dömötör, C. G. Hartinger, A. K. Bytzek, T. Kiss, B. K. Keppler, und E. A. Enyedy, „Characterization of the binding sites of the anticancer ruthenium(III) complexes KP1019 and KP1339 on human serum albumin via competition studies“, *JBIC J. Biol. Inorg. Chem.*, Bd. 18, Nr. 1, S. 9–17, Jan. 2013, doi: 10.1007/s00775-012-0944-6.

[9] N. Cetinbas, M. I. Webb, J. A. Dubland, und C. J. Walsby, „Serum-protein interactions with anticancer Ru(III) complexes KP1019 and KP418 characterized by EPR“, *JBIC J. Biol. Inorg. Chem.*, Bd. 15, Nr. 2, S. 131–145, Feb. 2010, doi: 10.1007/s00775-009-0578-5.

[10] „Neuer Wirkmechanismus von Tumortherapeutikum entdeckt“. https://medienportal.univie.ac.at/presse/aktuelle-pressemeldungen/detailansicht/artikel/neuer-wirkmechanismus-eines-in-oesterreich-entwickelten-tumortherapeutikums-entdeckt/ (zugegriffen März 10, 2021).

[11] M. U. of Vienna, „Promising metallodrug candidate for tumour therapy | MedUni Vienna“, *Medical University of Vienna*. https://www.meduniwien.ac.at/web/en/ueber-uns/news/2021/news-im-maerz-2021/vielversprechender-metallhaltiger-wirkstoffkandidat-fuer-tumortherapie/ (zugegriffen März 09, 2021).

[12] D. Wernitznig *u. a.*, „First-in-class ruthenium anticancer drug (KP1339/IT-139) induces an immunogenic cell death signature in colorectal spheroids in vitro†“, *Metallomics*, Bd. 11, Nr. 6, S. 1044–1048, Juni 2019, doi: 10.1039/c9mt00051h.

[13] R. Gałązka, „MODERN ANALYTICAL METHODS IN ENVIRONMENTAL ANALYSIS – ICP-MS TECHNIQUE“, März 2011, doi: 10.13140/RG.2.1.3854.7686.

[14] „Wieberneit, Einsatz der ICP- Massenspektrometrie zur Multielementbestimmung in biologischen Proben, 2001“. Zugegriffen: Juli 14, 2020. [Online]. Verfügbar unter: https://ediss.sub.uni-hamburg.de/volltexte/2001/543/pdf/Disse.pdf.

[15] S. C. Wilschefski und M. R. Baxter, „Inductively Coupled Plasma Mass Spectrometry: Introduction to Analytical Aspects“, *Clin. Biochem. Rev.*, Bd. 40, Nr. 3, S. 115–133, Aug. 2019, doi: 10.33176/AACB-19-00024.

[16] M. Shah und J. A. Caruso, „Inductively coupled plasma mass spectrometry in separation techniques: Recent trends in phosphorus speciation“, *J. Sep. Sci.*, Bd. 28, Nr. 15, S. 1969–1984, 2005, doi: 10.1002/jssc.200500234.

[17] S. Theiner, „Pharmacokinetic and bioimaging studies of platinum-based anticancer complexes by ICP-MS and LA-ICP-MS“, phd, uniwien, wien, 2015.

[18] R. Thomas, *Practical Guide to ICP-MS: A Tutorial for Beginners, Third Edition*. CRC Press, 2013.

[19] D. Pröfrock und A. Prange, „Inductively Coupled Plasma-Mass Spectrometry (ICP-MS) for Quantitative Analysis in Environmental and Life Sciences: A Review of Challenges, Solutions, and Trends“, *Appl. Spectrosc.*, Bd. 66, Nr. 8, S. 843–868, Aug. 2012.

[20] J. H. Gross, *Mass Spectrometry: A Textbook*, 3rd ed. 2017.. Cham : Springer International Publishing : Imprint: Springer, 2017.

[21] D. Argoti, „Liquid chromatography : mass spectrometry for detection and characterization of DNA biomarkers and reactive metabolites“, *Chem. Diss.*, Dez. 2020.

[22] M. Wiedenbeck *u. a.*, „GGR Biennial Critical Review: Analytical Developments Since 2010“, *Geostand. Geoanalytical Res.*, Bd. 36, Nr. 4, S. 337–398, 2012, doi: https://doi.org/10.1111/j.1751-908X.2012.00218.x.

[23] I. V. Chernushevich, A. V. Loboda, und B. A. Thomson, „An introduction to quadrupole–time-of-flight mass spectrometry“, *J. Mass Spectrom.*, Bd. 36, Nr. 8, S. 849–865, 2001, doi: 10.1002/jms.207.

[24] J. O. R. Gustafsson, M. K. Oehler, A. Ruszkiewicz, S. R. McColl, und P. Hoffmann, „MALDI Imaging Mass Spectrometry (MALDI-IMS)—Application of Spatial Proteomics for Ovarian Cancer Classification and Diagnosis“, *Int. J. Mol. Sci.*, Bd. 12, Nr. 1, Art. Nr. 1, Jan. 2011, doi: 10.3390/ijms12010773.

[25] S. Medhe, „Mass Spectrometry: Detectors Review“, *Annu. Rev. Chem. Biomol. Eng.*, Bd. 3, S. 51–58, Okt. 2018, doi: 10.11648/j.cbe.20180304.11.

[26] E. Bolea-Fernandez, L. Balcaen, M. Resano, und F. Vanhaecke, „Overcoming spectral overlap via inductively coupled plasma-tandem mass spectrometry (ICP-MS/MS). A tutorial review“, *J. Anal. At. Spectrom.*, Bd. 32, Nr. 9, S. 1660–1679, Aug. 2017, doi: 10.1039/C7JA00010C.

[27] L. Balcaen, G. Woods, M. Resano, und F. Vanhaecke, „Accurate determination of S in organic matrices using isotope dilution ICP-MS / MS“, *J. Anal. At. Spectrom.*, Bd. 28, Nr. 1, S. 33–39, 2013, doi: 10.1039/C2JA30265A.

[28] „Comparison of ICP-QQQ and MP-AES to Alternative Atomic Spectrometry Techniques“. http://www.labcompare.com/10-Featured-Articles/333957-Comparison-of-ICP-QQQ-and-MP-AES-to-Alternative-Atomic-Spectrometry-Techniques/ (zugegriffen Dez. 14, 2020).

[29] C.-S. Hsiung, J. D. Andrade, R. Costa, und K. O. Ash, „Minimizing interferences in the quantitative multielement analysis of trace elements in biological fluids by inductively coupled plasma mass spectrometry“, *Clin. Chem.*, Bd. 43, Nr. 12, S. 2303–2311, Dez. 1997, doi: 10.1093/clinchem/43.12.2303.

[30] R. C. Machado, C. D. B. Amaral, D. Schiavo, J. A. Nóbrega, und A. R. A. Nogueira, „Complex samples and spectral interferences in ICP-MS: Evaluation of tandem mass spectrometry for interference-free determination of cadmium, tin and platinum group elements“, *Microchem. J.*, Bd. 130, S. 271–275, Jan. 2017, doi: 10.1016/j.microc.2016.09.011.

[31] D. Pick, M. Leiterer, und J. W. Einax, „Reduction of polyatomic interferences in biological material using dynamic reaction cell ICP-MS“, *Microchem. J.*, Bd. 95, Nr. 2, S. 315–319, Juli 2010, doi: 10.1016/j.microc.2010.01.008.

[32] N. Sugiyama und Y. Shikamori, „Removal of spectral interferences on noble metal elements using MS/MS reaction cell mode of a triple quadrupole ICP-MS“, *J. Anal. At. Spectrom.*, Bd. 30, Nr. 12, S. 2481–2487, Nov. 2015, doi: 10.1039/C5JA00308C.

[33] N. Yamada, „Kinetic energy discrimination in collision/reaction cell ICP-MS: Theoretical review of principles and limitations“, *Spectrochim. Acta*, Bd. 110, S. 31–44, Aug. 2015, doi: 10.1016/j.sab.2015.05.008.

[34] S. D. Fernández, N. Sugishama, J. R. Encinar, und A. Sanz-Medel, „Triple Quad ICPMS (ICPQQQ) as a New Tool for Absolute Quantitative Proteomics and Phosphoproteomics“, *Anal. Chem.*, Bd. 84, Nr. 14, S. 5851–5857, Juli 2012, doi: 10.1021/ac3009516.

[35] M. Wilm, „Principles of Electrospray Ionization“, *Mol. Cell. Proteomics*, Bd. 10, Nr. 7, Juli 2011, doi: 10.1074/mcp.M111.009407.

[36] C. Ho *u. a.*, „Electrospray Ionisation Mass Spectrometry: Principles and Clinical Applications“, *Clin. Biochem. Rev.*, Bd. 24, Nr. 1, S. 3–12, Feb. 2003.

[37] R. H. Perry, R. G. Cooks, und R. J. Noll, „Orbitrap mass spectrometry: Instrumentation, ion motion and applications“, *Mass Spectrom. Rev.*, Bd. 27, Nr. 6, S. 661–699, 2008, doi: https://doi.org/10.1002/mas.20186.

[38] C. Proteomics, „Q Exactive Hybrid Quadrupole-Orbitrap Mass Spectrometer“, *Creative Proteomics*. https://www.creative-proteomics.com/support/q-exactive-hybrid-quadrupole-orbitrap-mass-spectrometer.htm (zugegriffen Dez. 29, 2020).

[39] Q. Hu, R. J. Noll, H. Li, A. Makarov, M. Hardman, und R. Graham Cooks, „The Orbitrap: a new mass spectrometer“, *J. Mass Spectrom.*, Bd. 40, Nr. 4, S. 430–443, Apr. 2005, doi: 10.1002/jms.856.

[40] „PharmaWiki - Albumin“. https://www.pharmawiki.ch/wiki/index.php?wiki=Albumin (zugegriffen März 11, 2021).

[41] „16600 - McCoy’s 5A (modified) - AT“. https://www.thermofisher.com/at/en/home/technical-resources/media-formulation.83.html (zugegriffen Aug. 23, 2020).

List of tables

List of figures

6 Supporting Info

Table 27: Initial-, output weight and dilution factor of the blood pellets digestion procedure

Mice Blood pellets			
Sample	**Initial weight [mg]**	**Output weight [mg]**	**Dilution factor**
mouse 3_KP1339	10.91	9538.30	874.27
mouse 4_KP1339	23.95	9468.08	395.33
mouse 5_KP1339	14.12	9133.47	646.85
mouse 6_KP1339	7.28	8932.78	1227.03
mouse 7_control	16.79	8913.05	530.85
mouse 8_control	22.38	8870.52	396.36
mouse 13_etomoxir + KP1339	11.59	9148.34	789.33
mouse 14_etomoxir + KP1339	8.61	9410.40	1092.96
mouse 15_etomoxir + KP1339	13.21	8934.33	676.33
mouse 16_etomoxir+ KP1339	12.73	9035.45	709.78

Table 28: Stds for the determination of the Ru conc. in mice blood pellets (mouse 5-8, 13-16)

Standard name	Made of	Addition [µL]	Initial weight Ru[1)] [mg]	Addition acid[2)] [mL]	Output weight [mg]	c_{Ru} [ppb]	c_{Ru} [µg/L]
Single standard						990099.01	1000000.00
A1 10000	Single std.	100	105.00	9.9	10168.84	10223.43	10325.66
A3 100	A1 10000	100	103.91	9.9	10157.99	104.58	105.63
BLANK 1				10.0			
B 30	A3	3000	3064.69	7.0	10155.53	31.56	31.88
B 20	A3	2000	2055.83	8.0	10143.1	21.20	21.41
B 10	A3	1000	1025.04	9.0	10147.03	10.56	10.67
B 5	A3	500	512.59	9.5	10165.62	5.27	5.33
B 1	B10	1000	1019.76	9.0	10141.28	1.06	1.07
B 0.5	B10	500	509.27	9.5	10178.13	0.53	0.53
B 0.1	B1	1000	1019.69	9.0	10141.32	0.11	0.11
BLANK 2				10.0			

[1)] Ru 1000 ± 3 µg/mL in 10% HCl (Peak Performance)

[2)] 3% HNO_3 (Density 1.01 g/cm³)

Table 29: Stds for the determination of the Ru conc. in mice blood pellets (mouse 3, 4)

Standard name	Made of	Addition [µL]	Initial weight Ru[1)] [mg]	Addition acid[2)] [mL]	Output weight [mg]	c_{Ru} [ppb]	c_{Ru} [µg/L]
Single standard						990099.01	1000000.00
A1 10000	Single std.	100	101.13	9.9	10157.83	9857.29	9955.87
A 1000	A1	100	1017.61	9.0	10069.82	996.13	1006.09
BLANK 1				10.0			
B 30	A 1000	300	301.07	9.7	10146.27	29.56	29.85
B 20	A 1000	200	201.46	9.8	10141.31	19.79	19.99
B 10	A 1000	100	101.03	9.9	10158.06	9.91	10.01
B 5	A 1000	50	50.25	10.0	10151.85	4.93	4.98
B 1	B10	1000	1013.07	9.0	10149.79	0.99	1.00
B 0.5	B 5	1000	1011.76	9.0	10131.67	0.49	0.50
B 0.1	B1	1000	1015.15	9.0	10133.62	0.10	0.10
B 0.05	B 0.5	1000	1015.27	9.0	10160.05	0.05	0.05
BLANK 2				10.0			

[1)] Ru 1000 ± 3 µg/mL in 10% HCl (Peak Performance)

[2)] 3% HNO_3 (Density 1.01g/cm^3)

Table 30: Stds for the determination of the Ru conc. in mice blood serum samples

Standard name	Made of	Addition [µL]	Initial weight Ru[1)] [mg]	Addition acid[2)] [mL]	Output weight [mg]	c_{Ru} [ppb]	c_{Ru} [µg/L]
Single standard						990099.01	1000000.00
A1 10000	Single std.	100	103.24	9.9	10175.73	10045.26	10145.71
A3 100	A1	100	101.83	9.9	10168.62	100.59	101.60
BLANK 1				10.0			
B 30	A3	3000	3051.44	7.0	10144.07	30.26	30.56
B 20	A3	2000	2032.46	8.0	10155.34	20.13	20.33
B 10	A3	1000	1014.23	9.0	10156.54	10.05	10.15
B 5	A3	500	507.61	9.5	10151.43	5.03	5.08
B 1	B10	1000	1013.41	9.0	10141.57	1.00	1.01
B 0.5	B5	1000	1012.62	9.0	10148.45	0.50	0.51
B 0.1	B1	1000	1012.56	9.0	10138.20	0.10	0.10
BLANK 2				10.0			

[1)] Ru 1000 ± 3 µg/mL in 10% HCl (Peak Performance)

[2)] 3% HNO_3 (Density 1.01g/cm³)